Extracting informative spatio-temporal features from fMRI dynamics: A model-based characterization of timescales

Jessica De Santiago

TESIS DOCTORAL UPF / 2020

Thesis supervisor

Prof. Gustavo Deco

Department of Information and Communication Technologies

Universitat Pompeu Fabra Barcelona

Acknowledgment

Siempre recordaré el año 2020 y no solamente yo...

La humanidad entera se enfrenta en estos momentos a una de las pruebas más difíciles de supervivencia, una pandemia global que de diferentes maneras ha cambiado la vida de todos.

A pesar de la situación global, tengo que mencionar que he sido de las personas más afortunadas. Ahí afuera el mundo se detuvo exactamente en uno de los momentos en los que yo más necesitaba estar en casa escribiendo. Mientras todos echábamos de menos salir a tomar algo y abrazar a nuestros familiares y amigos, yo escapé del mundo escribiendo. El proceso no ha sido fácil, pero ha sido mucho más llevadero gracias a todas las personas que hicieron posible este sueño. A mis padres, a quienes les ha costado demasiado aceptar la idea de dejarme ir al otro lado del mundo; ha sido gracias a su amor y apoyo la que me trajo hasta este logro tan importante en mi vida. A mi hermana Elisa, de quien me siento muy orgullosa. Acepto que para mí ha sido doblemente difícil estar lejos de ustedes, pero no se preocupen no he estado sola:

Mi supervisor de doctorado, el Dr. Gustavo Deco, ha estado ahí en cada paso guiándome con su experiencia y conocimientos, apoyán-

dome hasta el último momento de enviar mi tesis y aun después. Irene, quien es mi compañera de generación, de despacho, de vida. Kalinka, a quien admiro infinitamente y se ha convertido en más que una amiga.

Andrea y Rob que han sido parte de esta nueva familia que me adoptó. Matt, ha sido mi segundo supervisor y un gran amigo. Vicente que ha estado ahí para hablar conmigo de Machine Learning, de ciencia, de tonterías, para escuchar mis quejas y mucho más que hablar. Ane, Laura, Manel, Katt, Sofia, Ana, mis compañeros del día a día que sin darse cuenta se volvieron pare importante de esta experiencia.

Mi parte de México, Montse y Angel, con quien siempre he podido disfrutar de la comida que tanto extraño de mi país.

Vero, Sandy, David, Pam y Paco, mis amigos que, aunque están repartidos por el mundo, parece que están al lado mío todo el tiempo, desde que estudiábamos juntos. Y a Philipp, quien ha sido un apoyo muy importante.

A todos ustedes, gracias por ser parte de este sueño hecho realidad y sobre todo por ser parte de mi vida.

Abstract

In neuropsychiatry, the development of brain imaging and dedicated data analysis for personalized medicine promises to predict both the evolution of diseases and responses of treatments. The ability to estimate the time course of the disease is the first step to understand the response to potential treatments, which implies the development of methods able to capture subject-specific features in addition to the discrimination between pathological conditions. However, methods that effectively characterize the neuronal activity at the whole-brain level are still lacking, and many efforts are currently made in the fields of clinical research and neuroscience to fill this gap. The above is particularly problematic to interpret functional Magnetic Resonance Imaging (fMRI) data, which are indirectly coupled with neuronal activity because of hemodynamics, yielding much slower signals than neuronal activity. We propose a multiscale method that combines a computational whole-brain model with machine learning to solve this issue. In our approach, the model relates the neuronal activity and the fMRI signals in a mechanistic fashion, allowing for access to neuronal activity down to millisecond precision. Specifically, we use a novel methodology that allows the extraction of space-time

motifs at different timescales through binned time windows. Then, we use machine learning to study which range of timescales in the modeled neuronal activity is most informative to separate the brain's dynamics during rest, distinguishing subjects, tasks, and neuropsychiatric conditions. To do so, we apply a classifier to the spatiotemporal activity patterns, spanning timescales from milliseconds to seconds. Our results show associations between conditions and brain activity patterns that are as specific between conditions as a fingerprinting. Our findings determined that the timescale that extracts the most particular features during rest and task is at around 200ms and slower for separating neuropsychiatric disorders (400ms); both timescales are much faster than that of fMRI signals. Our multiscale computational approach is a further step to study the multiple timescales of brain dynamics and predict the dynamical interactions between brain regions. Overall, this method raises outlooks to detect biomarkers and predict responses of treatments.

Keywords: whole-brain modeling; space-time motifs; machine learning; biomarkers; personalized medicine.

Resumen

En neuropsiquiatría, la aplicación de la medicina personalizada promete (entre otros beneficios) predecir tanto la respuesta a tratamientos, como el curso de las enfermedades, lo anterior basándose en características específicas de los pacientes. Sin embargo, en neurociencia prevalece la necesidad de desarrollar métodos que capturen de manera efectiva la actividad cerebral en un domino mamplio. Para lograrlo, proponemos un método multiescala que incorporen el modelado computacional y aprendizaje automático. En nuestro enfoque, estudiamos a partir de datos de imagen de resonancia magnética (fMRI por sus siglas en inglés), el rango de escalas de tiempo que extrae con precisión la información más específica para separar la dinámica cerebral en reposo, tareas y condiciones neuropsiquiátricas. Los datos fueron analizados aplicando un modelado computación de todo el cerebro, el cual incorpora actividad sináptica cerebral en milisegundos. Además, utilizamos una metodología que extrae patrones espaciotemporales a diferentes escalas de tiempo por medio de binning. A continuación, aplicamos un clasificador a estos patrones de actividad espaciotemporales, a diferentes escalas de tiempo, nuestros resultados muestran asociaciones entre condiciones y patrones de actividad

cerebral que son tan específicos entre condiciones como una huella dactilar. Nuestros resultados determinan que la escala de tiempo que extraen las características mas particulares, tanto durante reposo como en tarea es alrededor de 200ms, y más lento para separar condiciones neuropsiquiátricas (400ms), escalas que no son accesibles utilizando fMRI. Nuestro enfoque computacional multiescala puede ayudar a estudiar la dinámica cerebral en varias escalas temporales y así como a predecir las interacciones de la dinámica cerebral. En general, este método despierta expectativas para el entendimiento las características espaciotemporales de la dinámica cerebral y de trastornos neuropsiquiátricos, dicho conocimiento potencialmente podría ser aprovechado para detectar biomarcadores y aplicar intervenciones terapéuticas dirigidas.

Palabras claves: modelado computacional del cerebro completo; patrones espaciotemporales; aprendizaje automático; biomarcadores; medicina personalizada.

Contents

List of Figures

Chapter 1

Introduction

1.1 Overview

The present manuscript introduces a novel multiscale computational framework for studying human brain dynamics; this work's main contribution is a timescale characterization of the whole-brain. Such characterization is based on machine learning algorithms.

This work contributes to an emerging research field at the intersection of machine learning and timescale characterization of brain dynamics. It follows a constructive approach to get more insights into intrinsic brain dynamics, human cognition, and possible disruptions in neuropsychiatric conditions. Chapter 1 introduces personalized medicine fundamentals, benchmark methodologies for studying brain dynamics, and new approaches that analyze such dynamics at many timescales, particularly when integrated into a whole-brain

model. The following Chapter 2 details the multiscale methodology that we implement. The subsequent Chapters 3- 5 present three studies: firstly, a timescale characterization study of intrinsic brain dynamics, on which we aim to extract the most characteristic timescale for separating different subjects; next, we analyze the most specific timescale of cognitive-based brain dynamics; and last, we characterize across timescales different neuropsychiatric conditions. All these chapters rely on the decoding of subjects, tasks, or conditions to identify the most informative timescale. The last Chapter 6 sums up their contributions and puts them into context with the literature.

1.2 Characterizing function and structure of the human brain

Personalized medicine in neuropsychiatry, promises (among other benefits) the use of biomarkers to predict the pathogenesis of diseases as well as responses to treatments as well as, based on subject-specific features (Matthews et al., 2014; Hamburg and Collins, 2010; Polivka et al., 2016). The above mentioned implies the development of methods able to capture subject-specific features in addition to the discrimination between pathological conditions. Personalized medicine challenges neuroscience in finding methods for characterizing the neuronal activity at the whole-brain level (Brammer, 2009). However, to detect patterns in neuropsychiatric disorders, such as schizophrenia and bipolar disorder, it is fundamental first to have a better understanding of control subjects' dynamics; neural activity

has shown an intrinsic organization in both space and time that is far from being fully understood (Deco et al., 2011). Toward the concept of personalized care for neuropsychiatric disorders, remains the need for developing multiscale methods that effectively capture the neural dynamics of whole-brain (Markram, 2013).

Typically, imaging tools for the whole-brain are suited to data that reflect the behavior of a population of neurons, such as the electroencephalogram (EEG), magnetoencephalogram (MEG), and fMRI (Haines, 2012). However, these tools have both advantages and limitations; For example, MEG is a very costly tool because it is not widespread in clinics and is more used for research (Squire et al., 2013). In contrast, EEG is a widely used technique because it is comparatively cheap, but its spatial resolution is relatively low to uncover detailed brain networks involved in neuropathologies. On the other hand, both clinical and research applications commonly use MRI scanners to explore brain anatomy lesions; it is essentially due to its refined spatial resolution (Bandettini, 2009; Glover, 2011).

Traditional methodologies for studying brain connectivity

The information processing that underlies brain functions, such as learning and cognitive processes, emerges from the interaction of neuronal populations at both local and global scales (Bressler and Kelso, 2001; V. K. Jirsa, 2004; Bressler, 2002). For studying global brain mechanisms, it is needed to map whole-brain structure and function; in this line, we can use neuroimaging methodologies for estimating different topological and functional measures. Typically,

the mapping of neuroanatomical connections (figure1.1A) that can be expressed in terms of structural connectivity (SC) matrix, is possible by combining techniques such as MRI or diffusion tensor imaging (DTI) (Johansen-Berg and Rushworth, 2009; Hagmann et al., 2010). On the other hand, the tracking of brain function (see fig 1.1B) can be assessed using, for example, fMRI or echo-planar imaging (EPI); the functional connectivity (FC) comes from statistical correlations of brain activity between regions (V. K. Jirsa, 2004; Greicius et al., 2003).

For a better understanding of the fundamentals in brain dynamics and how this basis underlays complex brain functions, it is necessary the integration of experimental techniques at different levels, to incorporate as a whole: single neurons, neurophysiology, neuroanatomy and neuroimaging. In cognitive neuroscience, it is essential to capture the neural dynamics that are involved in the elaboration of cognitive processes.

Neuroimaging methods allow the study of brain activity across several temporal scales and with varying degrees of spatio-temporal resolution and invasiveness to the participant (figure1.2) (Lenartowicz and Poldrack, 2010). By applying these methods the association of neuronal activity with brain areas has been studied, both while performing a specific task as well as during resting-state (in the absence of a stimulus or task, hereafter called rs-MRI) (Fox and Raichle, 2007; Greicius et al., 2003). Studies of rs-MRI demonstrated that even at rest, there are common trends of neuronal activity across different subjects (Damoiseaux et al., 2006; Pannunzi et al., 2017). A recent study, which simultaneously used fMRI, positron emission to-

mography (PET) and EEG, found that such intrinsic dynamics are as specific as a fingerprint and that, based on resting-state activity alone, it is possible to discriminate among different participants (Shah et al., 2017). This ability to decode subject-specific information from measured brain activity is a strong indication that we can identify trait-dependent features of spontaneous brain activity. The identification of individual traits promises great expectations for defining neural disorders more precisely, as well as for identifying predictive biomarkers (Polivka et al., 2016; Dickerson et al., 2011) and for the application of personalized medical interventions (V. K. Jirsa et al., 2017).

To overcome the experimental difficulties of measuring brain signals with a single technique, a computational whole-brain model can be used to simulate both neural activity and its performance in the inaccessible spatiotemporal range (Deco and Kringelbach, 2014; Deco et al., 2008).

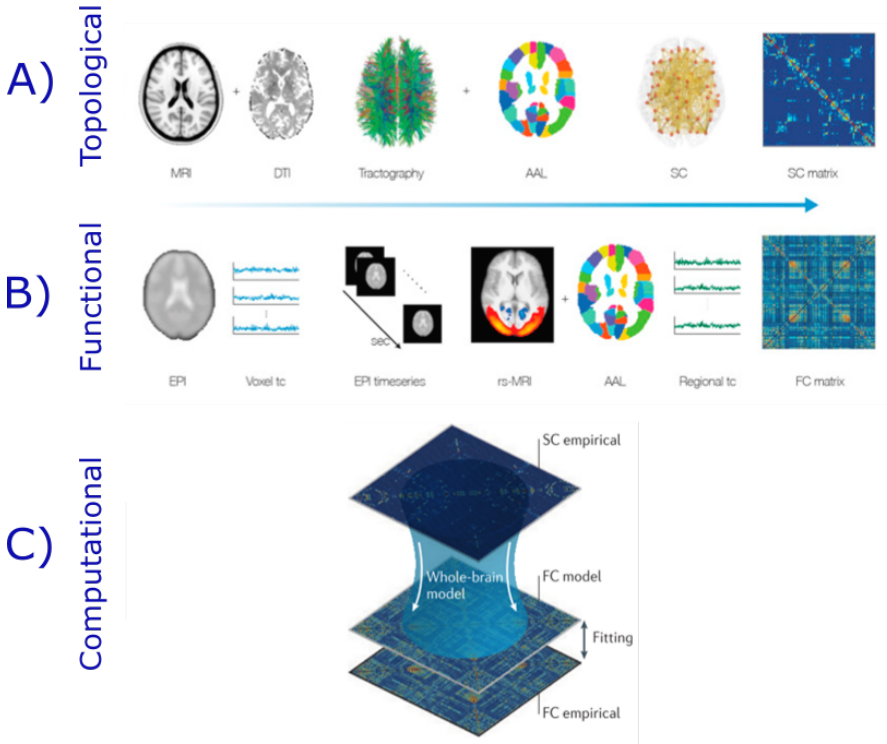

Figure 1.1: Overview of methods for mapping structure and brain activity. **(A)** As represented schematically, for estimating the structural connectivity (SC) matrix that represents anatomical connections, we combine topological measuring such as; structural MRI, DTI and tractography. We use the topological measures together with a parcellation template, here the automatic anatomical labeling (AAL). **(B)** Regarding the functional connectivity (FC) matrix, we measure brain activity using methods such as fMRI and EPI, for example, by analyzing resting-state data (rs-MRI) with the AAL parcellation scheme and correlating the time courses between regions. **(C)** On the other hand, Whole-brain computational models reproduce brain function using empirical data (SC and FC respectively), the optimal working point for the model is at which modelled FC and empirical FC match. This scheme is adapted from Deco, Hartevelt, et al., 2017

.

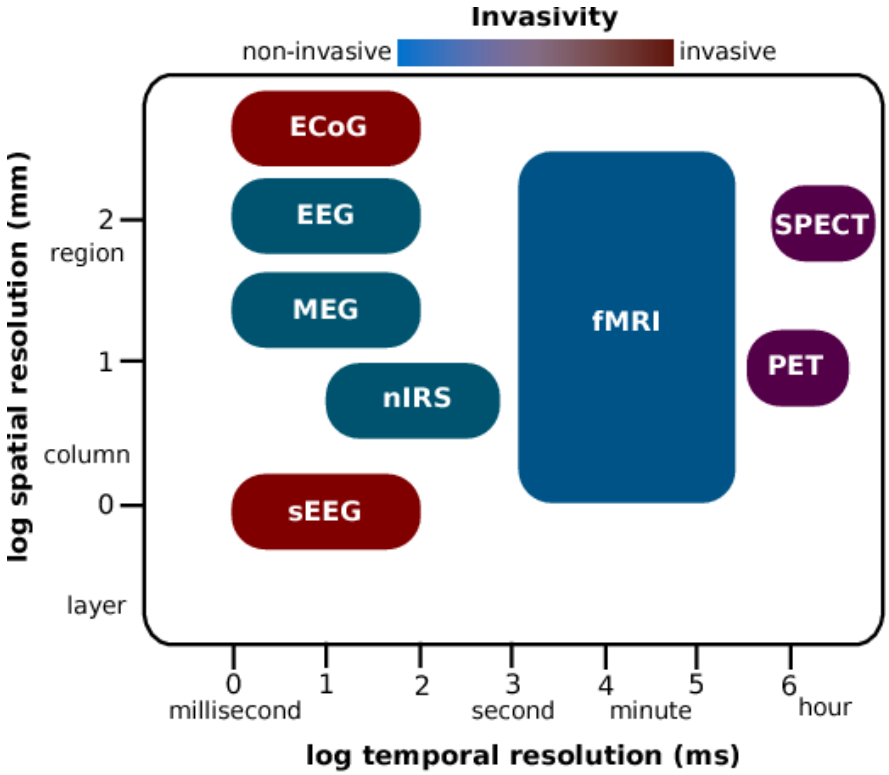

Figure 1.2: Resolution of various functional neuroimaging methods. In this graph, each colored area represents an estimation of the spatial (y-axis) and temporal resolution (x-axis) of a neuroimaging methodology. The heat map denotes the invasiveness of the method, where the lowest value is blue (non-invasive) and the highest value dark red (invasive). Notice that the fMRI is a non-invasive technique that reaches a broad spatial domain; nevertheless, its temporal resolution is limited to seconds (1-3 seconds). Abbreviations: ECoG, electrocorticography; EEG, electroencephalography; MEG, magnetoencephalography; nIRS, functional near-infrared spectroscopy; fMRI, functional magnetic resonance imaging; SPECT, single-photon emission computed tomography; PET, positron emission tomography; Adapted from Idrobo, 2017

1.3 Modelling brain dynamics

Computational modeling has raised great expectations for understanding both healthy brain dynamics and its possible disruptions in neuropsychiatric disorders (Deco and Kringelbach, 2014; Fan and Markram, 2019; Wass, 2011). As figure 1C displays, whole-brain models link empirical SC and FC to reproduce, as the output of the model (modelled FC), some of the dynamics and complexity of the brain.

How can computational models help us to understand the fundamental mechanisms of neural processes? More importantly, how can neuroscientist relate these neural processes to neuroscience data? In the following, we review a variety of computational frameworks that have been used for measuring brain dynamics via neuroimaging.

Starting from single neurons, neurons are the computing elements of brain dynamics, reason why it becomes necessary starting computational modeling from at the single neuron level. Cortical neurons are cells that can produce impulses or spikes called action potentials with high timing and precision, such an accurate organization may have an important role for encoding, transmitting and integrating signals in the nervous system (Mainen and Sejnowski, 1995). It is possible to characterize action potentials in terms of their timing and frequency (i.e., temporal and rate coding respectively). The computation of activity in populations of neurons can be described reducing the large population of spiking neurons, to a function that describes the distribution of neural states at a given time. Such function can be further reduced to a single variable that describes the average firing rate.

The modeling of such mechanisms is relevant in neuroscience for describing processes that are not directly observable, such as the case of mean-field models of neuronal dynamics. Mean-field models capture important aspects of neuronal function such as both inhibitory and excitatory interactions to reflect the average behavior of a population of neurons.

1.3.1 Mean-field model

The mean-field approximation is a standard method used in statistical physics: it considers many individual components and describes their average behavior. This principle has been used to develop mathematical models that reproduce the mean activity in neural populations. Mean-field models aim to find the right mathematical description that captures the effect of individual (local) properties at the population level. As figure 1.3 shows, these models consider essential components of brain dynamics such as neuronal functions and their interactions (e.g., intracellular, receptors) which are essential for reflecting, for example, the temporal relationship between neural elements.

The application of mean-field approximations into whole-brain models, combined with neuroimaging might might contribute to reach resolutions that are not accessible using a single neuroimaging technique (Fan and Markram, 2019). In previous work, Deco and colleagues proposed the novel "Brain Songs framework" to extract spacetime motifs (Deco et al., 2019); these motifs are sets of brain regions (also called brain assemblies) that are able to synchronize their activity in both space and time. The framework aims at identi-

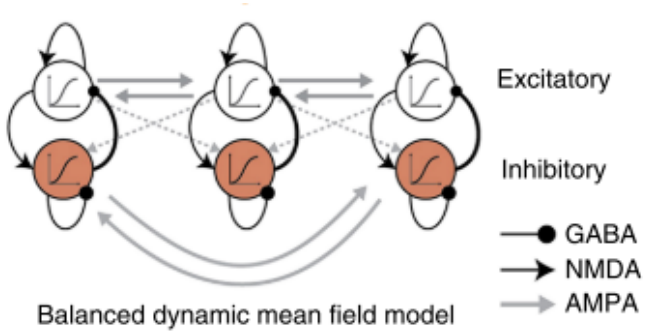

Figure 1.3: Representation of a Mean-field model for describing brain dynamics. The mean-field approximation mathematically describes the effect of individual (local) properties at the population level. These models consider essential components of brain dynamics such as neuronal functions and their interactions (e.g., intracellular, receptors). This figure represents a dynamic mean-field model that considers both excitatory (mediated by NMDA) and inhibitory synaptic currents (mediated by GABA-A). In this representation, the inhibitory pools connect with the excitatory pools (only locally), while long-range connections link the excitatory pools. Adapted from Deco et al., 2019

fying groups of brain regions with co-activation patterns and tracking this activity at many timescales by applying a computational model.

1.4 Brain assemblies as a measure of space-time motifs

The concept of brain assemblies comes from the translation of neural assemblies from spiking neurons, to the interactions between different brain regions at the whole-brain level. Neuronal assemblies also called cell-assemblies (see *Neuronal assemblies*) are sets of neurons that interact with other groups of neurons; correlations of temporal patterns of spikes give this interaction. The hypothesis of neural orga-

nization in cell assemblies has been studied in hippocampal neurons (**reinagel2002**) as well as their possible organization in time (Harris et al., 2003) (figure 1.4 includes cell assembly activity in the hippocampus from Harris et al., 2003).

Neuronal assemblies

The psychologist, Donald Hebb explored the possible synchronized cooperation of neurons, as a base for the processing of information; establishing that the neurons may be organized in groups, or cell assemblies (Hebb, 1949).

Hebb purposed specific cell assembly properties that could explain the neuronal code and his high efficiency:

- Overlapping: The same neuron may be part of different assemblies, which implies that the same neuron may be used in different processes at the same time (Sakurai, 1999). Moreover, this property suggests that there may be more cell assemblies than single cells in the brain (Sakurai, 1999).

- Dynamic connections: These connections allow functional interactions between assemblies, giving rise to changes when the information processed changes (Sakurai, 1999).

In the line of studying brain assemblies, empirical studies showed that in normal conditions, neural assemblies are dynamically arranged in space and time. Conversely, an imbalance between neuronal assemblies may lead to pathological states; such as schizophrenia, a mental disorder that has been related to a disbalance between large-scale integration of spatiotemporal patterns (reference).

For translating cell assemblies at whole-brain dynamics, we base our work on Deco's approach that conceptualizes the organization of brain activity from the hierarchy an entropy of cortical assemblies (Deco et al., 2019) (see 1.5); considering brain dynamics as a complex hierarchy of brain regions that are organized in assemblies and interact with other assemblies or sets of regions, in both space and time.

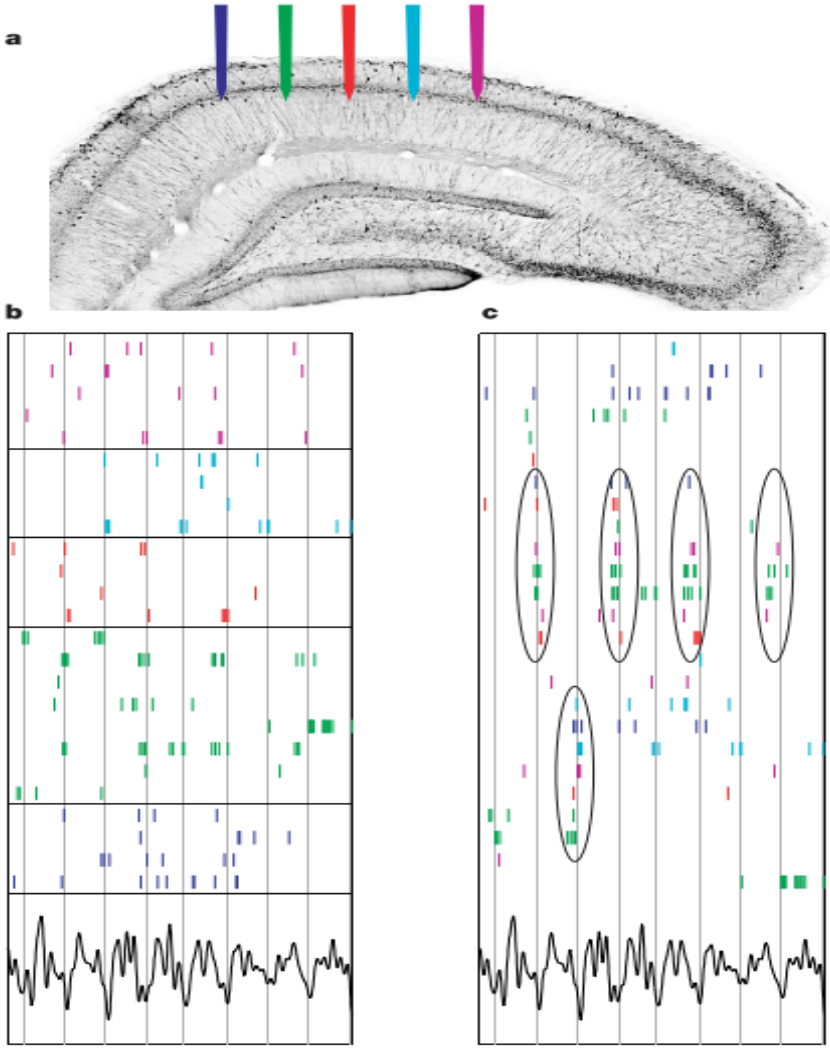

Figure 1.4: Organization of cell assemblies in the hippocampus from Harris et al., 2003. In the investigation of Harris (with rats) (Harris et al., 2003), he demostrates how the pyramidal cells are organized in cell assemblies. In this figure he shows **a)** the location of electrodes that record simultaneously hippocampal cells (25 cells during 1s). **b)** the ordering of neurons according to their physical position represented in colour-code and vertical lines indicate troughs of theta waves (bottom trace). And **c)** the reordered spike raster to highlight synchrony (circled) between anatomically distributed populations. Such organization is called 'cell assemblies'. Figure from Harris et al., 2003

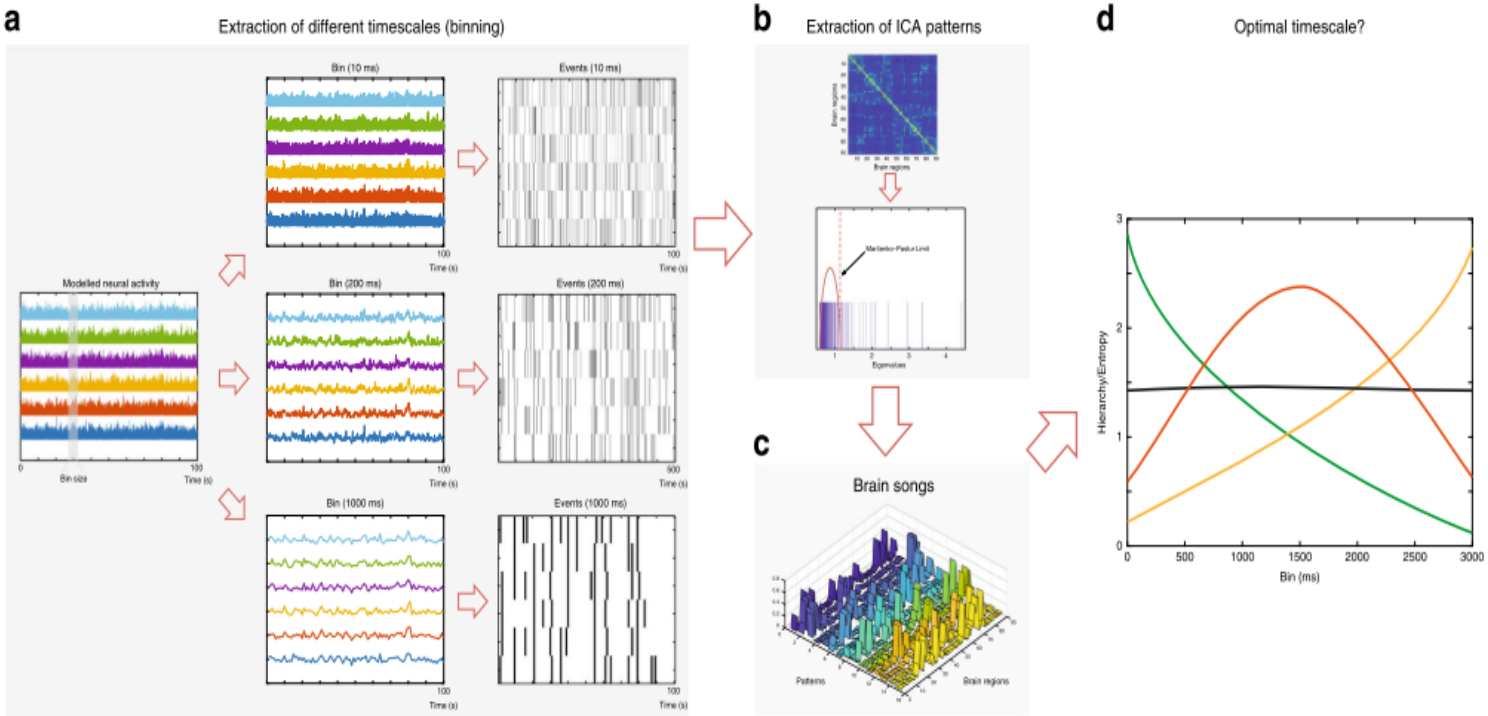

Figure 1.5: Brain assemblies measured with entropy and hierarchy of functional whole-brain organization from Deco et al., 2019. In Deco's work, he applies the brain assemblies' approach for studying whole-brain dynamics and measures across time both entropy and hierarchy of these spatiotemporal structures as follows; **A)** First, the creation of different bin sizes at 10, 200, 1000ms, respectively, of the milliseconds neural time series. Followed by the binarization of the time binned time series. After **B)** the extraction of the number of significant spacetime motifs using independent component analysis and the estimation of brain assemblies' activity. **D)**Displays the richness of the dynamical repertoire measured with entropy and hierarchy at different timescales; this varies across timescales whether flat, monotonic decrease or increase or having an optimum. Figure from Deco et al., 2019

1.5 Machine learning for decoding cognitive conditions, identifying functional networks and extracting biomarkers

In neuroscience, the potential of combining whole-brain modeling with machine learning tools for understanding healthy brain dynamics as well as neuropsychiatric syndromes is probably one of the most important perspectives (Glaser et al., 2019; Lemm et al., 2011). Machine learning focuses on the generation of algorithms that can learn from existing data and, based on the learned patterns, make predictions about new data (Varoquaux and Thirion, 2014). An example in the field of neuroscience could be to predict a categorical output, such as a specific neurological disease (Glaser et al., 2019). By implementing machine learning, we could get some leads for biomarkers, as well as personalized diagnoses and prognoses.

1.5.1 Cognitive applications

Cognitive neuroscientists are still a long way from understanding how the brain works (Vacariu and Vacariu, 2013). If researchers can design simple algorithms to identify patterns of brain activity while performing a specific task, it would provide a baseline for testing more complex cognitive theories (Carlson et al., 2018). We can implement simple machine learning tools such as classification to give us preliminary explanations about the neural underpinnings of complex cognitive functions such as reasoning or learning (Holzinger, 2014;

Janssen et al., 2018).

1.5.2 Personalized Medicine

Personalizing treatments based on individual-brain features, also called stratified medicine, has long been fundamental to neurology (Matthews et al., 2014; Ozomaro et al., 2013). For practicing stratified based neuroscience, it is crucial to develop methods that characterize the richness of brain dynamics at many levels of its organization (Markram, 2013). By combining multiple brain imaging techniques, for example simultaneous recording of fMRI and EEG, it is possible to reach a more extensive spatiotemporal domain than using a single method as none of the existing neuroimaging techniques can capture brain activity on both a broad spatial and temporal scale simultaneously (**UllspergerM.&Debener2010**; Mulert et al., 2008). However, it is still not well understood which spatiotemporal scales are most relevant during spontaneous brain activity, and multimodal approaches are costly and prone to artefacts (Steyrl et al., 2015).

1.5.3 Predictive neuroscience leading to potential Biomarkers

Biomarkers are biological signatures that can be used as an indicator of normal processes, pathological processes, or responses to pharmacological treatments (Strimbu and Tavel, 2010; Filiou and Turck, 2011). By applying machine learning tools, it has been possible to

bridge theoretical neuroscience with clinical applications by refining the ways we make predictions (**WooC.&Wager2017**) and identified useful biomarkers in neuroimaging data of neuropsychiatric patients (Akzhigitov et al., 2018; Janssen et al., 2018).

1.6 Promises of integrating whole-brain modeling and machine learning

In this work, we present a multiscale approach that integrates computational modelling for accessing neuronal dynamics, with the mapping of dynamic patterns of brain activity as well as machine learning. This approach aims to uncover the most distinctive spatiotemporal domain of brain dynamics from a classification perspective, from which we examine the classification performance to separate three different classes; individuals, cognitive tasks and neuropsychiatric disorders. First, we apply a computational whole-brain model, that recovers neural signals at the millisecond timescale from both the underlying structural connectivity and functional brain dynamics measured using fMRI. This was followed by the application of the "Brain assemblies" method, which extracts co-activation patterns of brain regions across temporal scales, from milliseconds to seconds (Deco et al., 2019). Subsequently, we implement a multinomial logistic regression (MLR) classifier to predict the target class (e.g., subjects, cognitive tasks and neuropsychiatric conditions) based on brain activity. We examine the classifier accuracy based on the space-time motifs in comparison with benchmark methods such as functional con-

nectivity (FC; which calculates whole-brain activity based on static spatial correlations). The classifier is applied across timescales to identify the most informative spatiotemporal domain for separating between conditions.

Chapter 2

Methodology

Our analysis pipeline is displayed in Fig 2.1. We fit a modified dynamic mean field (DMF) model (Deco et al., 2014) to blood oxygenation level dependent (BOLD) signals from fMRI data. This model is then used to generate the neuronal dynamics at a shorter timescale, which is subsequently estimated using the brain assemblies framework (Deco et al., 2019). In the present manuscript, the co-activation patterns of brain assemblies are then fed into a classifier, that is based on multinomial logistic regression and k-nearest-neighbor, to discriminate three different classes; subjects, tasks and neuropsychiatric disorders.

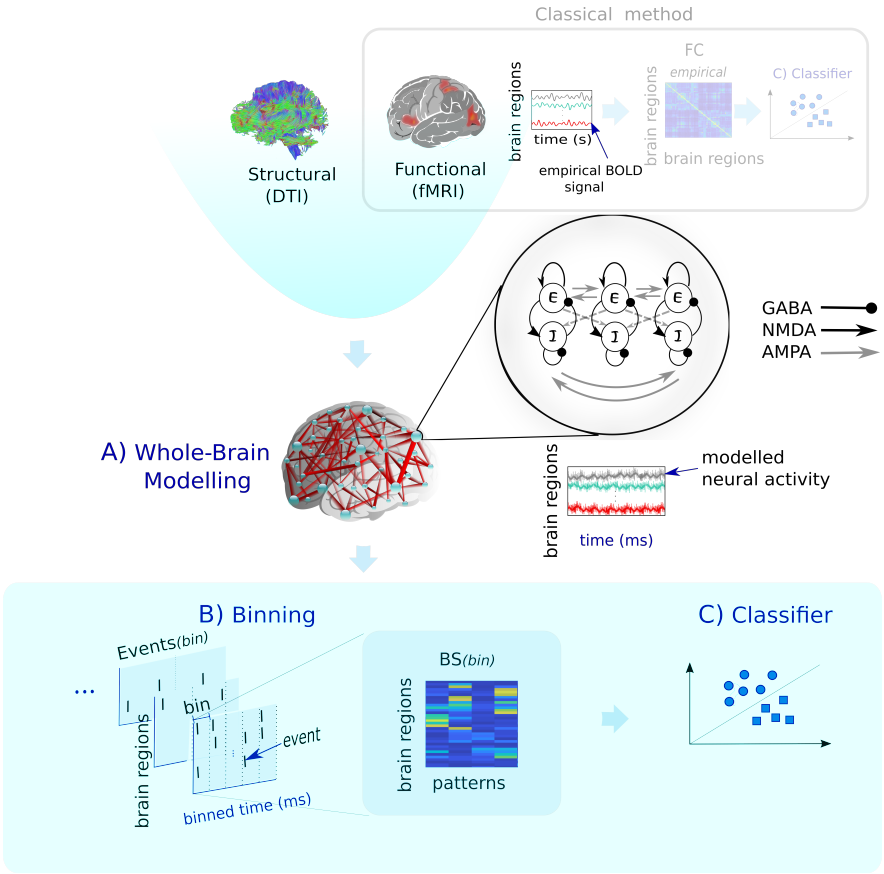

Figure 2.1: Illustration of the general methodology used in this study briefly described three steps. The methodology of this study can be summarized as follows; the implementation of **(A)** Whole-brain modelling of BOLD signals, to recover the intrinsic neurodynamical time-series (in milliseconds). Followed by the **(B)** Binning of the modelled output, where time windows are created from milliseconds to seconds, in order to extract the spacetime motifs$_{(bin)}$ at many timescales. Lastly, the implementation across binned timeframes of the **(C)** classifier to the space-time motifs$_{(bin)}$, for capturing the particularity of each condition (different individuals, tasks and neuropsychiatric disorders) across time.

2.1 Acquisition and preprocessing of neuroimaging data (empirical data)

The present study aims to uncover the temporal scale (or range of temporal scales), which reflects the most distinctive signature of whole-brain spatiotemporal dynamics. We restrict our study to whole-brain measures that estimate the correlated activity between brain regions or subsets of brain regions (i.e. FC and space-time motifs, respectively). Explicitly we explored the whole-brain dynamical distinctiveness in three different views; firstly, we explore the whole-brain signature in a context to distinguish among different subjects, secondly, we investigate this signature to differentiate separated cognitive conditions (i.e. resting, working memory), and finally to discriminate various neuropsychiatric disorders (such as schizophrenia and bipolar disorder). To examine such perspectives, we analyzed three datasets; the first dataset incorporates several sessions from subjects resting during each session (resting-state data (Zuo et al., 2014)). Second, a dataset that includes sessions where subjects performed different cognitive tasks (task-related dataset (Senden et al., 2017)). The third dataset comprises rs-fMRI of healthy participants as well as participants with neuropsychiatric diagnoses (neuropsychiatric conditions dataset (Poldrack et al., 2016)); a brief summary of the description of these datasets is in table 2.1. In the following, we describe the technical information of such datasets.

Table 2.1: Summary of the description of the datasets analyzed in this study. We explored the whole-brain dynamical distinctiveness of three different classes: subjects, cognitive tasks and neuropsychiatric conditions. To examine such perspectives, we analyzed the three datasets that are listed in this table.

Dataset	Condition (s)	Subjects	Notes
Resting-state (Zuo et al., 2014)	rs-fMRI	30	Healthy controls, 10 sessions
Tasks-related (Senden et al., 2017)	rs-fMRI, visual n-back task (Kirchner, 1958) executive flanker task (Eriksen and Eriksen, 1974), mental rotation (Shepard and Metzler, 1971) and odd-man-out task (Flowers and Robertson, 1985).	14	Healthy controls, one session of each task
Neuropsychiatric conditions (Poldrack et al., 2016)	rs-fMRI	265	Healthy controls (130 subjects), participants with; schizophrenia (50 subjects), ADHD (43 subjects) and bipolar disorder (49 subjects).

2.1.1 Resting-state data

The dataset analyzed in this study was obtained from the publicly available compilation of the Consortium for Reliability and Reproducibility (CoRR) (Zuo et al., 2014). This CoRR dataset comprises ten resting-state fMRI scans, each with a duration of 10 minutes, from thirty healthy subjects. Each subject accomplished the recording sessions within a month, attending fMRI scans every three days (always around a similar time of day).

fMRI data acquisition

Scanning sessions were carried out at Hangzhou Normal University using a GE MR750 3T scanner (GE Medical Systems, Waukesha, WI). During scans, participants were presented with a screen displaying a central fixation point. Additionally, they were instructed to relax without falling asleep, to maintain their eyes open and not to think of anything in particular. To minimize head motion of each participant, foam cushions and straps were used to fix the head comfortably.

Functional resting-state data were obtained using a T2-weighted BOLD-sensitive gradient-echo echo-planar imaging [EPI] with repetition time [TR]=2000ms; echo time [TE]=30ms; flip angle [FA]=90°; field of View [FoV]=220x220mm2; matrix 64x64; voxel size=3.4x3.4x3.4mm3; 43 slices. For coregistration, anatomical scans were obtained with a sagittal T1-weighted, Fast Spoiled Gradient Echo (FSPGR) sequence scan with the following protocol: TR=8.1ms; TE=3.1ms; TI=450ms; FA= 8°; FoV =256x256; voxel

size =1x1x1mm3; 176 sagittal slices.

Structural connectivity

For determining anatomical connections, we used a generic matrix that denotes the structural relationships between any pair of brain areas and , and that follows the AAL parcellation with regions of interest (ROIs) -50-. To estimate a neuro-anatomical connectivity matrix we use, for each participant, white matter tractography between pairs of cortical areas. Further, we average the matrices over subjects and apply a threshold for the existence of connections. We additionally consider interhemispheric connections by adding all possible connections between ROIs that mirror both hemispheres. Such associations have demonstrated relevance in whole-cortex modelling of BOLD activity (Messé et al., 2014) and are not captured using only tractography (Hagmann et al., 2008).

Preprocessing

Imaging preprocessing of functional data was carried out with SPM12 (Wellcome Trust Centre for Neuroimaging, London, UK) and DPARSF/DPABI (Yan et al., 2016). The pipeline comprised slice-timing correction, realignment for motion correction and co-registration of the T1 anatomical image to the mean functional image. Moreover, preprocessing included detrending, regression of 6 movement parameters, five principal component analysis (PCA), white matter and cerebrospinal fluid (CSF) with the application of compo-

nent based method (CompCor) (Behzadi et al., 2007) for the reduction of noise in BOLD data, as well as spatial normalization to MNI coordinates. Furthermore, scrubbing with Power 0.5 and linear interpolation were performed. The parcellation of this dataset consists of 116 ROIs after pooling voxels into ROIs based on automated anatomical labelling (AAL) (**tzourio2002**). Finally, ROI time courses were band-pass filtered in the range between 0.01 and 0.08 Hz.

2.1.2 Task-related dataset (one rest condition and four cognitive tasks)

This dataset analyzed is composed of ten sessions of resting-state (described in more detail by Senden et al. Senden et al., 2017), which includes data from fourteen healthy subjects in five behavioral conditions. These conditions consist of a resting-state session (without any task and with eyes closed) and four different tasks which were selected to reflect a specific cognitive function such as; working memory (visual n-back task (Kirchner, 1958)), executive function inhibition (Eriksen flanker task (Eriksen and Eriksen, 1974)), mental rotation (Shepard and Metzler, 1971) and semantic reasoning (verbal odd-man-out task (Flowers and Robertson, 1985)). Each task lasted roughly seven minutes while resting-state lasted eight minutes, and all conditions consisted of 192 volumes of 2 seconds.

fMRI data acquisition

All imaging data were acquired at Maastricht Brain Imaging Centre (Maastricht University) on a Siemens 3T scanner (Tim Trio upgraded to Prisma Fit). Anatomical images were collected with a rapid acquisition gradient-echo T1-weighted MPRAGE image (192 sagittal slices; TR=2250ms; TE=2.21ms; FA=9°; FoV=256×256 mm2; 1 mm isotropic resolution). Followed by the acquisition of functional images, that was performed using an EPI sequence that comprised 38 transversal slices with TR=2000ms, TE=30ms, and FA =77° (voxel size=3×3×3.5 mm^3); no slice gap; GRAPPA=3.

Preprocessing

Anatomical data preprocessing was carried out automatically using FreeSurfer (Reuter et al., 2012)(http://surfer.nmr.mgh.harvard.edu/) and the probabilistic atlas parcellation described by the Desikan Killany (DK) cortical atlas (Desikan et al., 2006). Regarding functional images, its preprocessing was performed in two sections, firstly using BrainVoyager QX (v2.6; Brain Innovation, Maastricht, the Netherlands) for slice scan time correction, 3D-motion correction, a high-pass cutoff filtering of 0.01 Hz and registration of both functional and anatomical images respectively. Previous steps followed by cleaning the signals in MATLAB (version 8.10.0. Natick, Massachusetts: The MathWorks Inc., 2013) using wavelet de-spiking (Patel and Bullmore, 2016) and regressing out a global noise signal as determined by the first principal component of signals observed in the ventricles. Finally, the average BOLD signal for each of 68 cortical regions defined

by the DK atlas (Desikan et al., 2006) was computed.

2.1.3 Neuropsychiatric conditions dataset

In this chapter, we apply our multiscale framework to study a set of neuropsychiatric conditions. We analyze 265 participants (ages between 21-50 years) from the UCLA Consortium for Neuropsychiatric Phenomics (CNP) dataset (Poldrack et al., 2016). From the CNP dataset, we analyze a subset that comprises resting-state fMRI data (which scans lasted 304s), each with structural T1-w; of both healthy (130 subjects) and patient groups. The clinic population include neuropsychiatric syndromes such as; schizophrenia (50 subjects), participants with adult Attention Deficit Hyperactivity Disorder (ADHD) (43 subjects) and bipolar disorder (49 subjects).

fMRI data acquisition

Data were acquired at the Ahmanson-Lovelace Brain Mapping Center in a 3T Siemens Trio scanner (Siemens version syngo MR B15). fMRI data were collected with a T2*-w EPI sequence with the following parameters: slice thickness = 4mm, 34 slices, TR=2s, TE=30ms, flip angle=90°, matrix=64 × 64, FOV=192mm. MPRAGE and a T1-w high-resolution anatomical scan were collected; TR=1.9s, TE=2.26ms, slice thickness = 1mm, 176 slices, matrix=256 × 256, FOV=250mm. DWI data were acquired with: TR/TE=9000/93ms, slice thickness = 2mm, 64 directions, flip angle=90°, matrix=96 × 96, axial slices, b=1000s/mm2.

Preprocessing

The preprocessing of the neuropsychiatric conditions dataset 45 was performed using the preprocessing pipeline for fMRIpipelines called fMRIPrep (Esteban et al., 2019). Our approach of such preprocessing comprises two sections: the first is carried out with (a) fMRIprep v1.1.1 (Esteban et al., 2019), a Nipype-based tool (Gorgolewski et al., 2011); and next, the (b) denoising using the iterative correction method called Diffuse Cluster Estimation and Regression (DiCER).

fMRIprep workflow Each T1-weighted (T1w) volume was corrected for intensity non-uniformity through N4BiasFieldCorrection v2.1.0 (Tustison et al., 2010) and skull-stripped using antsBrainExtraction.sh v2.1.0 (with the NKI template). Brain surfaces were reconstructed using recon-all from FreeSurfer v6.0.1 (Dale et al., 1999). A brain mask was estimated with FreeSurfer, which was refined using an atlas based brain mask, similar to that within Klein et al., 2017. Spatial normalization to the ICBM 152 Nonlinear Asymmetrical template version 2009c (Fonov et al., 2009) was performed through nonlinear registration with the ants- Registration tool of ANTs v2.1.0 (Avants et al., 2008), using brain-extracted versions of both T1w volume and template. Brain-tissue segmentation of cerebrospinal fluid (CSF), white-matter (WM) and gray-matter (GM) was performed on the brain-extracted T1w using fast (Zhang et al., 2001) (FSL v5.0.9).

Functional data were slice-time corrected using 3dTshift from AFNI v16.2.07 (Cox, R.W. and Hyde, 1997) and realigned to a mean ref-

erence image using mcflirt (Jenkinson et al., 2002). 'Fieldmap-less' distortion correction was performed by co-registering the functional image to the intensity-inverted T1w image (Huntenburg, 2014; Wang et al., 2017) constrained with an EPI distortion atlas (Treiber et al., 2016) and implemented with antsRegistration (ANTs). While this approach requires rigorous, systematic validation, we have found that it visually improves coregistration between anatomical and functional images. This was followed by co-registration to the corresponding T1w using boundary-based registration (Greve and Fischl, 2009) with nine degrees of freedom (bbregister within FreeSurfer v6.0.1). The motion-correcting transformations, field-distortion-correcting warp, BOLD-to-T1w transformation, and T1w-to-template (MNI) warp were concatenated and applied in a single step using antsApply Trans- forms (ANTs v2.1.0) (Lanczos, 1964). Framewise displacement was calculated for each functional run using the implementation of Nipype (Power et al., 2014). ICA-based Automatic Removal Of Motion Artifacts (AROMA) was used to generate noise regressors for use in the non-aggressive variant of the method (Pruim et al., 2015).

Post-fMRIprep processing (denoising) After the preprocessing using fMRIprep (Esteban et al., 2019), we use DiCER (Aquino et al., 2020) for removing diverse kinds of widespread signal deflection, and inter-subject variability in global correlation structure. DiCER algorithm identifies the most characteristic signals that are directly related to large clusters of coherent voxels (Aquino et al., 2020), following we describe the methods of this denoising scheme in terms of the outputs from fMRIprep v1.1.1 58 (details at https://github.com/

BMHLab/DiCER).

As the next step of the fmriprep pipeline, the fMRI data were analyzed within the MNI 152 Asymmetric 2009c space, fMRI data and remaining anatomical images were resampled to the native BOLD imaging dimensions. The automatically labeled noise and BOLD ICA components from ICA-AROMA (described in the previous section "2.1.3fMRIprep workflow") were used to perform a non-aggressive variant of ICA-AROMA on the unsmoothed outputs of this pipeline. Regressors were calculated on the spatially smoothed variant as described in the preprocessing pipeline (6 mm FHWM kernel) and then applied to the unsmoothed preprocessed file.

In what follows, for minimizing partial-volume effects, the analysis was restricted to voxels contained within the GM voxels probability masks (with a threshold at >50% probability). Finally, to avoid contamination by voxels with low signal plagued by susceptibility and partial-volume effects, the voxels with signal intensities below 70% of the mean fMRI signal intensity were excluded.

2.2 Estimation of empirical FC

We measured the static correlations of the fMRI BOLD time series, of all conditions, through the FC measure. Such FC measures were calculated by the Pearson correlation coefficients between all pairs of brain regions, from ongoing fluctuations in empirical fMRI BOLD time series. As result of the previous calculations, and according to the parcellation scheme of each dataset, we generate FC symmetric

matrices with dimensions; 116×116 (116 regions ROIs -50-) for each scan of the resting-state data (Zuo et al., 2014); 68×68 (68 ROIs from DK cortical atlas; Desikan et al., 2006) regarding each session of the task-related dataset (Senden et al., 2017); And 82×82 concerning each rs-fMRI session of the neuropsychiatric conditions.

2.3 Whole-brain computational modelling

2.3.1 Dynamic Mean-field Model

Mean-field models have been widely used for modeling neural responses (Deco and Rolls, 2005), fMRI activation patterns and effects of pharmacological agents (Wilson et al., 2006). Here, we modelled brain dynamics at a timescale of milliseconds, based on the structural connectivity of brain regions; by applying a reduced version of a whole-brain mean-field model (DMF) (Deco et al., 2014) (Figure 2.1.A) that incorporates neuronal noise (Wong and Wang, 2006). The DMF approach establishes that the dynamic of brain regions is given by interconnected excitatory-inhibitory sub-networks (E–I networks). This model considers NMDA receptors and GABA-A receptors as mediators of excitatory and inhibitory synaptic currents, respectively. Sub-networks interact both within a brain region as well as between areas; at the local level, excitatory currents link with inhibitory pools, whereas excitatory pools of different areas are associated by long-range connections determined by the structural connectivity matrix C_{ij}.

In this version of the DMF model, we used rate-constants at the millisecond scale, together with real neurophysiological values from the Wong and Wang (Wong and Wang, 2006) derivation, who based their model on the original spiking neural network of Brunel and Wang (Brunel and Wang, 2001). More concretely, we can describe the model with the following differential equations:

$$I_i^{(E)} = W_E I_0 + w + J_{NMDA} S_i^{(E)} + G J_{NMDA} \sum_j C_{ij} S_j^{(E)} - J_i S_i^{(I)} \tag{2.1}$$

$$I_i^{(I)} = W_I I_0 + J_{NMDA} S_i^{(E)} - S_i^{(I)} + \lambda G J_{NMDA} \sum_j C_{ij} S_j^{(E)} \tag{2.2}$$

$$r_i^{(E)} = H^{(E)}(I_i^{(E)}) = \frac{\alpha_E I_i^{(E)} - b_E}{1 - exp(-d_E(\alpha_E I_i^{(E)} - b_E))} \tag{2.3}$$

$$r_i^{(I)} = H^{(I)}(I_i^{(I)}) = \frac{\alpha_I I_i^{(I)} - b_I}{1 - exp(-d_I(\alpha_I I_i^{(I)} - b_I))} \tag{2.4}$$

$$\frac{dS_i^{(E)}(t)}{dt} = -\frac{S_i^{(E)}}{\tau_E} + (1 - S_i^{(E)})\gamma r_i^{(E)} + \sigma v_i(t) \tag{2.5}$$

$$\frac{dS_i^{(I)}(t)}{dt} = -\frac{S_i^{(I)}}{\tau_I} + \gamma r_i^{(I)} + \sigma v_i(t) \tag{2.6}$$

Where $I_i^{(E,I)}$ are input currents to the excitatory (E) or inhibitory (I) population in the isolated brain region (i), both currents are set by the overall effective external input $I_0 = 0.382$ (nA) along with the suitable values of $W_{(E,I)}$, and excitatory synaptic coupling $J_{(E,I)}$), for obtaining a low level of spontaneous activity in the area. We used Feedback inhibition control (FIC) (Deco et al., 2014) to model a more realistic evoked activity of the network, by adjusting as table 2.2 shows, the values of $W_{(E,I)}$ and $J_{(E,I)}$ respectively. With such settings, we clamp the mean firing rate of the excitatory pool to 3Hz in a local network $G = 0$. Furthermore, $S_i^{(E,I)}$ represents the average synaptic gating, while $w = 1.4$ is the local excitatory recurrence.

In Eq. 2.3 and 2.4, $r_i^{(E,I)}$ indicates the population firing rate of either excitatory (E) or inhibitory pools. $r_i^{(E,I)}$ is defined by the neuronal input-output functions $H^{(E,I)}$, that convert the incoming input currents $I_i^{(E,I)}$into firing rates. We estimated $H(E, I)$ using the pyramidal cells values from Wong and Wang, 2006 , see table 2.2. Regarding Eqs. 2.5 and 2.6 $\gamma = \frac{0.641}{1000}$, where the divisor indicates rate-constants in the millisecond range, as well as $\tau_E = 100$ (ms) and $\tau_I = 10$ (ms). Moreover, v_i is uncorrelated standard Gaussian noise with an amplitude of $\sigma = 0.01$ (nA).

The inter-area connection weights between excitatory pools are given by the neuroanatomical matrix C. This matrix is scaled by the only free parameter of the model, the global coupling factor G, that equally scales all excitatory synapses. We adjusted the G parameter to move the modelled system to its optimal working point, which is the maximum fitting between simulated and the empirical functional dynamics. This adjustment fits the grand averaged static FC and the spa-

tiotemporal fluctuations in terms of their metastability (see *metastability*). We consequently assume that all regions present equal dynamics and that the conductivities of the coupling of each connecting fibre tract is also equivalent.

Metastability

In this work, we refer to metastability as a measure of the states' variability of phase configurations (as a function of time); it refers to how the synchronization between the different nodes fluctuates across time (Deco and Kringelbach, 2016). Thus, in our analysis, metastability is measured as the standard deviation of the Kuramoto order parameter across time (see section 2.3.4).

Table 2.2: Parameters of DMF. Parameter values for the neuronal response from Wong and Wang (Wong and Wang, 2006), and fixed values from the reduced version of such model Deco et al., 2014

NMDA excitatory (E) gating	GABA inhibitory (I) gating
$\mathrm{W}_E = 1$	$\mathrm{W}_I = 0.7$
$\mathrm{J}_E = 0.15(nA)$	$\mathrm{J}_I = 1(nA)$
$\mathrm{a}_E = 310(VnC)$	$\mathrm{a}_I = 615(VnC)$
$\mathrm{b}_E = 125(Hz)$	$\mathrm{b}_I = 177(Hz)$
$\mathrm{d}_E = 0.16(s)$	$\mathrm{d}_I = 0.087(s)$

2.3.2 Transforming neuronal activity into BOLD signal

We applied the hemodynamic Balloon–Windkessel (Friston et al., 2003; Stephan et al., 2007) model to the simulated excitatory synaptic activity $S^{(E)}$to obtain simulated fMRI blood oxygenation level-dependent (BOLD) signals. The Balloon–Windkessel model calculates the BOLD-signal in a brain area based on its neural activity, by

the summation of both excitatory and inhibitory populations (in this study, spiking activity is on the order of milliseconds). For the i-th region, z_i rises the vasodilatory signal s_i. The inflow f_i increases proportionally to the s_i signal, and these increments cause changes in both blood volume v_i and deoxyhemoglobin content q_i respectively. Biophysical variables and corresponding equations are the following:

$$\frac{ds_i}{dt} = 0.5r_i^{(E)} + 3 - ks_n - \gamma(f_n - 1) \tag{2.7}$$

$$\frac{df_i}{dt} = s_i \tag{2.8}$$

$$\frac{\tau dv_i}{dt} = f_i - v_i^{\alpha-1} \tag{2.9}$$

$$\frac{\tau dq_i}{dt} = \frac{f_i(1-\rho)^{f_i^{-}1}}{\frac{\rho - q_1 v_1^{\alpha-1}}{v_1}} \tag{2.10}$$

where the factor of resting oxygen extraction is indicated by ρ, and based on the modification presented by Deco and colleagues (Deco et al., 2019). In Eq. 2.7 the firing rate z_i for different conditions is within the experimental range. B_i is the BOLD signal of area i, which is a static nonlinear function of the volume of such region v_i, and deoxyhemoglobin is a volume-weighted sum of extra- and intravascular signals that can be represented as:

$$B_i = V_0[(k_1(1-q_1) + k_2(1-\frac{q_i}{v_1}) + k_3(1-v_1))] \tag{2.11}$$

Biophysical parameters of Eq 2.11 were taken from Stephan et al., 2007. Empirical as well as simulated BOLD signals were both band pass filtered between 0.1Hz and 0.01Hz, a range where resting- state activity is has been shown to be most functionally relevant (Biswal et al., 1995; Glerean et al., 2012; Achard et al., 2006).

2.3.3 Synchrony of BOLD signal oscillations

As a measure of the global level of synchronization, we used the Kuramoto synchronization index. In particular, by measuring the mean of the Kuramoto order parameter across time. First, we extracted the phases of the fMRI time series of each of the brain regions. Subsequently, we used the Hilbert transform (HT) on the filtered BOLD signals to extract the narrowband signal at time t, $\alpha(t)$, as a rotating vector with an instantaneous phase $\varphi(t)$, and an instantaneous amplitude $A(t)$. The phase and the amplitude are given by the argument and the modulus, respectively, of the complex signal $z(t)$, given by $z(t) = a(t) + j.\ HT[a(t)]$, where j is the imaginary unit. Finally, to calculate the global level of phase synchrony, we use the Kuramoto order parameter $R(t)$, that is expressed by:

$$R(t) = \frac{|\sum_k^n = 1^{ei\varphi k(t)}|}{n} \tag{2.12}$$

In Eq 2.12, n is the number of brain regions in the model. In this

work and according to the data $n = brainregions$. R represents the phase coherence of the system at time t and ranges between 1 (perfect synchrony) and 0 (complete asynchrony).

2.3.4 The Kuramoto order parameter

The Kuramoto order parameter, that as shown in previous work, is excellent for constraining the dynamical working point of fitting between whole-brain models and empirical data (Deco, Kringelbach, et al., 2017). By calculating the difference between the synchronization index (mean of Kuramoto parameter) and the empirical FC, is possible to find the optimal working point of the parameter G of the model, which is the point of maximal fitting of both simulated and empirical functional dynamics.

2.3.5 Fitting empirical and modeled data

We used the Kuramoto order parameter, that as shown in previous work, is excellent for constraining the dynamical working point of fitting between whole-brain models and empirical data85. We calculate the difference between the synchronization index (mean of Kuramoto parameter) and the empirical FC, to find the optimal working point of the parameter G of the model, which is the point of maximal fitting of both simulated and empirical functional dynamics.

At this point, the simulated neural activation matrix $brain\ regions \times time$ points (output of DMF model) denotes the brain region i (rows)

at a given time t at millisecond resolution (columns).

2.4 Access to different timescales through binning

2.4.1 Construction of event matrix at binned timescales

Binning simulated neural activity

To capture the contrast of brain dynamics across several timescales, we applied the framework by Deco and colleagues Deco et al., 2019, which translates a methodology to detect neuronal assemblies from spike data (Lopes-dos-Santos et al., 2011; Lopes-dos-Santos et al., 2013), into a whole-brain perspective and extracts subsets of brain regions with significant co-activation patterns. Adopting this approach, we binned the simulated neural activity (with dimensions $brainregions \times t$) at different timescales, where the bin width defines the timescale of the neuronal activity. In detail, we explored the temporal domain, from milliseconds to seconds, using bin sizes from 10 to 4000ms (increasing each window 10ms).

Over timescales between 10-4000ms we averaged the simulated time series within each time bin and then created binary 0,1 sequences. Such binarization was accomplished based on Tagliazucchi's (Tagliazucchi et al., 2012) method and the intrinsic ignition approach (Deco

and Kringelbach, 2017), by z scoring the averaged time series, where $Z_n(t_{bin})$ is the z-scored and averaged simulated activity of the brain region i in a time bin t_{bin}, and fixing the standard deviation as the threshold to define the events. Thus, having an event $\sigma_n(t_{bin})$=1 if $Z_n(t_{bin}) > \theta$ and $\sigma_n(t_{bin}) = 0$ (no event) otherwise. As a result of this binarization, we generate the event matrices in each time bin ($event_{bin}$ matrices), such that rows represent brain regions and columns the binned time.

2.5 Identification of spatiotemporal Motifs in binned timescales

2.5.1 Determination of the number of spacetime motifs at different timescales

Next, to extract brain assemblies over timescales ($space - timemotifs_{bin}$), we estimated the number of significant eigenvalues of $event_{bin}$ arrangements. The latter is obtained by applying Marčenko–Pastur distribution (Marchenko and Pastur, 1967), as shown in previous works (Wong and Wang, 2006; Lopes-dos-Santos et al., 2013; Deco et al., 2019). In detail, the number of spacetime motifs is given by the number of singular values (from event matrices) that are above Marčenko–Pastur distribution, which establishes that the eigenvalues of a normal random matrix M (with statistically independent rows) are given by the probability function:

$$p(\lambda) = \frac{q}{2\pi\rho^2}\frac{\sqrt{\lambda_{max} - \lambda)(\lambda - \lambda_{min}}}{\lambda} \tag{2.13}$$

Whit $q = N_{columns}/N_{rows} \geq 1$, where $N_{columns}$ and N_{rows} are the number of columns and rows of the matrix M. ρ^2 denotes the variance of the elements in M, while λ_{max}, λ_{min} are maximum and minimum bounds respectively, that are calculated by:

$$\lambda_{min}^{max} = \rho^2(1 \pm \sqrt{1/q})^2 \tag{2.14}$$

After this calculation, we homogenized the number of spacetime motifs within each bin size by averaging the number of patterns (rounded toward the next integer).

2.5.2 Extraction of brain assemblies

Finally, to extract the spatiotemporal patterns of co-activation, we conducted an ICA analysis, separately for each timescale. Specifically, we applied the Fast ICA algorithm (Peyrache et al., 2010) (in this work by using the FastICA toolbox for MATLAB http://research.ics.aalto.fi/ica/fastica/) to the $event_{bin}$ arrangements, where each significant component denotes a brain assembly, and the number of components is the average that we calculated in the previous section.

2.6 Classification

2.6.1 Reordering of the spatiotemporal structures

In this work, we applied a machine learning classifier (based on logistic regression) to find the timescale that captures the most specific signature of spatiotemporal brain dynamics for discriminating different conditions (subjects, tasks, neuropsychiatric conditions). To implement the classification, we first created more comparable arrays from the spatiotemporal structures ($brain\ assemblies_{bin}$) matrices). Since these spatiotemporal structures are co-activated patterns obtained through independent component analysis, the ordering of the patterns (i.e., columns of the $brain\ assemblies_{bin}$ arrangements) does not modify the components. Therefore, we rearranged the ordering of these patterns (horizontal axis of $brain\ assemblies_{bin}$ based on the ordering of the first session (as a reference of order); specifically, we computed the Pearson correlation coefficient (PCC) to calculate the similarity between the reference patterns and the patterns of all subjects and sessions (Figure 2.2A gives an example of this reordering). Finally, we rearranged the patterns (x-axis of the $brain\ assemblies_{bin}$ matrices) of all sessions in each timescale (10-4000ms), as determined by the ordering producing the highest correlation with the reference.

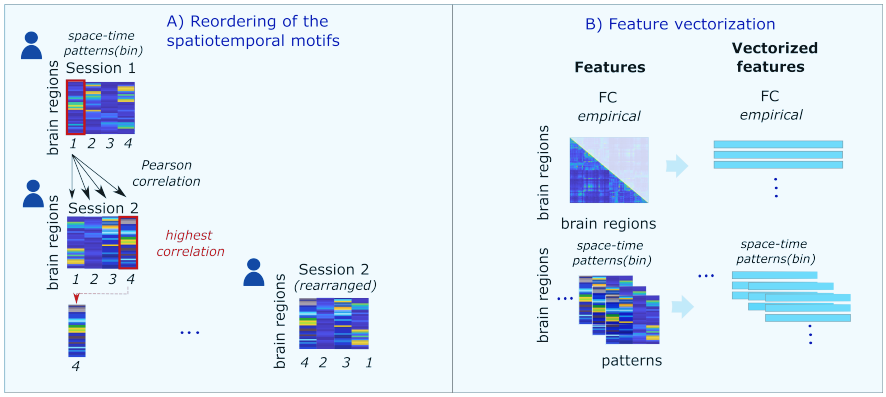

Figure 2.2: Illustration of the steps to perform the classification across timescales. To calculate across timescales, the classification within-subjects, firstly, we create more comparable arrays from the spacetime patterns, by **(A)** Reordering of the spatiotemporal structures, based on the order of the first session, we rearrange the patterns (columns of space-time motifs$_{(bin)}$ matrices) within-subjects. Next, **(B)** Feature vectorization by transforming into vectors the spatiotemporal structures and the lower triangle of the FC, respectively.

2.6.2 Feature vectorization

From the features extracted across subjects, i.e the empirical FC and space-time motifs$_{(bin)}$ measures, we structured the feature vectors as follows. Regarding the symmetrically weighted FC matrices, we obtained the feature vectors from the lower triangular part of each matrix (Figure 2.2B). On the other side, the space-time motifs$_{(bin)}$ matrices (brain regions × number of co-activation patterns) were directly vectorized after the reordering explained in the previous section (see sect. 2.6.1 'Reordering of the spatiotemporal structures'). After such vectorization, the resulting FC vectors comprise p=6670 features for the parcellation with n=116 ROIs 50 (resting-state data (Zuo et al., 2014)); p=2278 features for n=68 ROIs (Desikan et al., 2006) (tasks-related dataset (Senden et al., 2017)); and p=3321 re-

garding n=82 ROIs (data of neuropsychiatric conditions (Poldrack et al., 2016)). However, the number of spatiotemporal features differs across timescales since the number of spacetime motifs may differ across timescales. Consequently, the number of space-time motifs$_{(bin)}$ features also differs as a function of the number of co-activation patterns for a given time bin, e.g. $p = 1160$ using both the 116 brain regions and with the number of patterns equal to ten. Notice that we use the average number of space-time motifs$_{(bin)}$ (of all sessions and subjects) at a given timescale, see details in text for 2.5.1"Determination of the number of spacetime motifs".

2.6.3 K-nearest neighbors and Multinomial logistic regression algorithms

We apply the k-nearest neighbors algorithm to discriminate between individuals of the rs-fMRI data. This method implements similarity-based learning depending on the K nearest training examples (neighbors) of each query point (Varoquaux and Thirion, 2014).

On the other hand, we use a classification algorithm that is based on multinomial logistic regression to separate both tasks and neuropsychiatric conditions. Multinomial logistic regression is a linear model that trains using a subset of the data to predict the target classes, which, in this work, are tasks and neuropsychiatric disorders. Multinomial logistic regression classifier is a canonical tool for high-dimensional classification, the regressors of this model are adjusted in order to predict the probabilities of the sample, to be classified to each target category (i.e., tasks, conditions). Such probability relies

on the following function:

$$Pr(v^l \in S) = \phi(\sum_i w_i^s v_i^l) \tag{2.15}$$

Where v^l are the vectorized features (i.e., vectorized brain assemblies), i represents the index of each element for condition l to be in the target class s. ϕ is the sigmoid function (ranging from 0-1). The training of the classifier is performed by a regression to find the classification weigh w_i^s therefore that $Pr(v^l \in S)$ distinguishes the class s against the last class s^l.

We split the data into training and testing datasets to avoid overfitting. More specifically, we use one task/neuropsychiatric condition for learning the parameters of a predictive model, while the remaining sessions are used to evaluating the model (that is shown in fig. 2.3). We use a K-fold cross-validation scheme that repeatedly divides the data into k non-overlapping subsets, where k=number of subjects. For more reliable estimation of model performance, we randomly repeat the cross-validation 100 times and calculate the mean. To estimate the model assessment, we calculate the average from the accuracy scores of all repetitions. As the input of the classifier, we use either dynamic space-time motifs at different timescales or static FC as input, which arrays have the shape [samples × features].

Recursive feature elimination (RFE)

We applied the RFE template based on previous studies to extract effective whole-brain connectivity on the basis of related cognitive

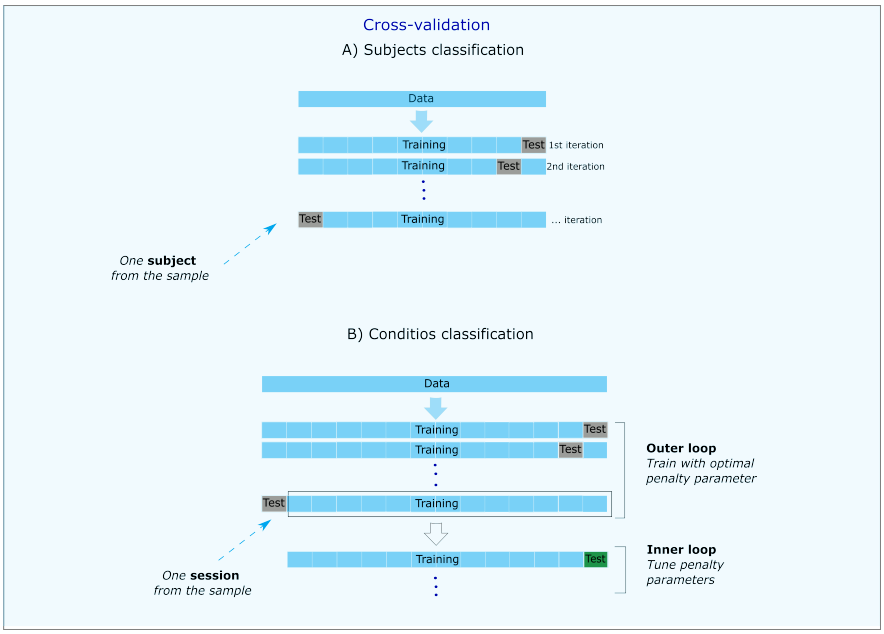

Figure 2.3: Cross-validation method. The data was divided into train and test sets (repeating 100 times). **(A)**) In terms of subject identification, we analyzed the resting-state dataset (Zuo et al., 2014), we train the classifier with one subject and test it using the rest of the sample (nine participants). **(B)** On the other hand, regarding tasks (Senden et al., 2017) and neuropsychiatric condition identification (Poldrack et al., 2016), we implement nested cross-validation, whit a train set of one session and a test set with the remaining sessions of the sample.

functional connectivity features (Stulz et al., 2018). From this previous study, in terms of cognitive distinctiveness, we implemented on the five conditions dataset, two cross-validation loops (see figure 2.3B), also known as nested cross-validation, to optimize the penalty parameter. Following the nested cross-validation, the cross-validation was formed by an outer loop of 14-folds, trained with thirteen of the fourteen subjects from the sample. Next, from the mentioned training set, the inner loop was trained with twelve of the thirteen subjects. Both loops of the nested cross-validation were tested with the remainder of one left-out subject.

All of the above is implemented in Python v3.7 using NumPy and SciPy libraries for numerical and mathematical analysis (http://www.scipy.org), respectively. For machine-learning we use the Scikit-learn library Pedregosa et al., 2011 (http://scikit-learn.org).

2.6.4 Similarity matrices between sessions and its contrast across timescales

After classifying participants using the dynamic patterns of brain activity as input, we explore the individuality of these features at each timescale. We use the PCC as a measure of similarity between sessions of all participants to examine the heterogeneity of different sessions. For such calculation, we create similarity matrices whose entries denote the PCC between the first session and the second session of the spatiotemporal features of each participant. Next, in order to measure how far was the second candidate with the most similar patterns, we compare them within each timescale by estimating the dif-

ference between the highest PCC value and the second-highest PCC. Further, this difference was measured per row (y-axis of similarity matrix) and averaged.

Chapter 3

Study 1: Individual signature of intrinsic brain dynamics

The present study aims to explore across timescales the distinctiveness of brain dynamics in different healthy and pathological brain states. For this purpose, we analyze datasets of three experimental studies within the same multiscale methodological framework (see 2.Methodology for details). These studies are; a) resting-state study, b) task-related study and c) neuropsychiatric study. Details of each of these studies are described in the section 2.1"Acquisition and preprocessing of neuroimaging data (empirical data)" section, for in-depth technical details review provided references.

In the following we describe the findings of our analyses, starting from the resting-state study. The resting brain state constitutes a reference baseline of brain dynamics, the multiscale study of co-activation patterns of spontaneous activity during rest state could pro-

vide a priori hypotheses about the most relevant timescale, or range of timescales, for extracting a signature of brain dynamics.

3.1 Introduction

In neuropsychiatry, the application of stratified medicine promises (among other benefits) to predict both responses of treatments and course of diseases, based on subject-specific features including biomarkers (Matthews et al., 2014, Hamburg and Collins, 2010, Polivka et al., 2016). Subject-based medicine challenges neuroscience in finding methods that capture the most specific brain features (Brammer, 2009). However, to detect patterns in neurological disruptions, it is fundamental first to have a better understanding of healthy brain dynamics; neural activity has shown an intrinsic organization in both space and time, that is far from being fully understood (Deco et al., 2011). Toward the concept of a personalized care for neurological diseases remains the need for developing multiscale methods that effectively captures individualized brain activity in a broad domain (Markram, 2013).

Studies of functional magnetic resonance imaging (fMRI) have demonstrated that even at rest, there are common trends of neuronal activity across different subjects (Damoiseaux et al., 2006, Pannunzi et al., 2017). A recent work which simultaneously used fMRI, positron emission tomography (PET) and electroencephalography (EEG), found that such intrinsic dynamics are as specific as a fingerprint that, based on resting-state activity alone, discrimi-

nate among different participants (Shah et al., 2017). This ability to decode subject-specific information from measured brain activity is a strong indication that we can identify trait-dependent features of spontaneous brain activity. The identification of individual traits promises great expectations for defining neural disorders more precisely, as well as for identifying predictive biomarkers (Polivka et al., 2016, Dickerson et al., 2011) and for the application of customized medical interventions (V. K. Jirsa et al., 2017).

For facing future approaches in stratification based neuroscience, it is crucial to develop methods that characterize the richness of brain dynamics at many levels of its organization (Markram, 2013). By combining multiple brain imaging techniques, for example simultaneous recording of fMRI and EEG, it is possible to reach a more extensive spatiotemporal domain than using a single method as none of the existing neuroimaging techniques can capture brain activity on both a broad spatial and temporal scale simultaneously (**UllspergerM.&Debener2010**, Mulert et al., 2008). However, it is still not well understood at which spatiotemporal scale spontaneous brain activity operates, and multimodal approaches are costly and prone to artefacts (Steyrl et al., 2015).

To overcome the experimental difficulties of measuring brain signals with a single technique, a computational whole-brain model can be used to simulate both neural activity and its performance in the inaccessible spatiotemporal range. In previous work, Deco and colleagues proposed the novel "Brain Songs framework" to extract spacetime motifs (Deco et al., 2019); these motifs are spatiotemporal and dynamical structures across the brain. The framework aims

at identifying groups of brain regions with co-activation patterns and tracking this activity at many timescales by applying a computational model.

In this study, we use machine learning to uncover the most distinctive spatiotemporal domain of brain dynamics from a subject classification perspective. Figure 3.1 displays the analysis pipeline, for details see chapter 2. First, we apply a computational whole-brain model, that recovers neural signals at the millisecond timescale from both the underlying structural connectivity and functional brain dynamics measured using fMRI. Followed by the implementation of the "Brain assemblies" method across temporal scales, which extracts the co-activation patterns of brain regions from milliseconds to seconds. After that, we implement a multinomial logistic regression (MLR) classifier to separate different subjects. In our approach, we characterize individuals' brain dynamics in terms of spatiotemporal structures in comparison with benchmark methods such as functional connectivity (FC; which calculates whole-brain activity based on static spatial correlations). The classifier is applied across timescales to identify the most informative spatiotemporal domain for separating different participants.

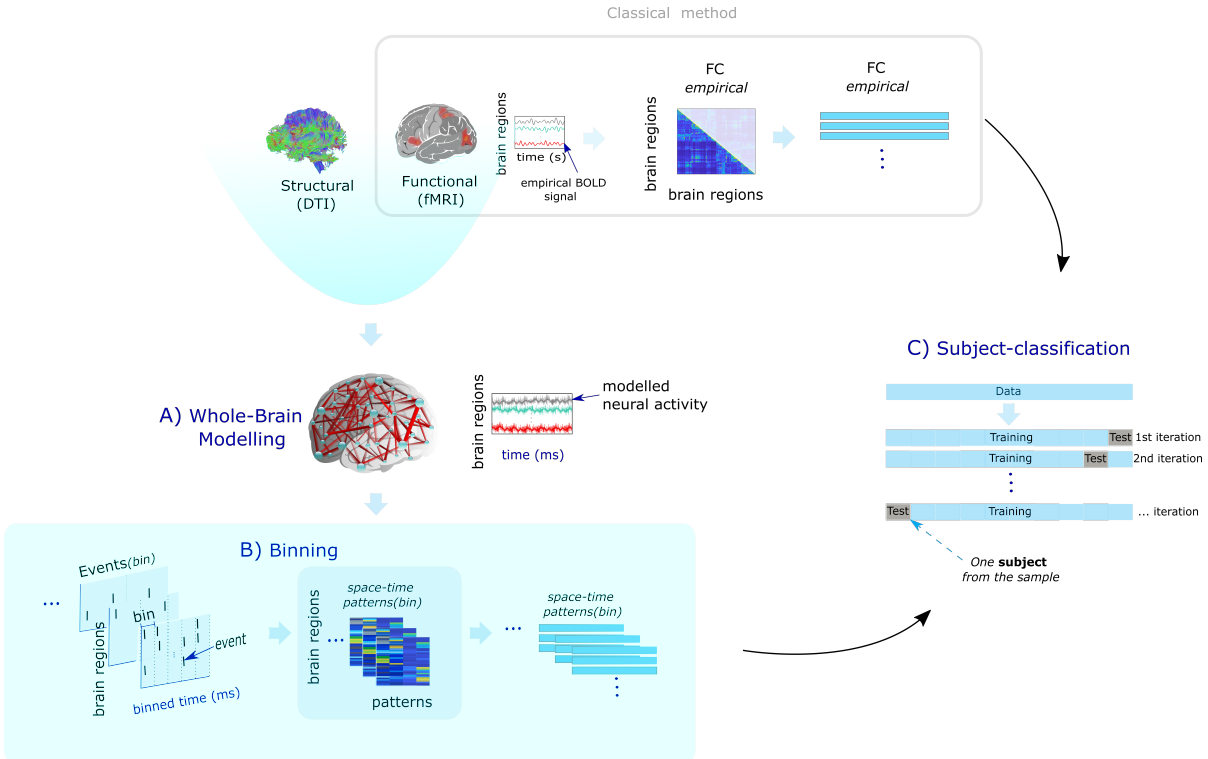

Figure 3.1: Subject-identification pipeline . Figure 1 displays the analysis pipeline of this study. **A)** We fit the dynamic mean-field (DMF) model to BOLD signals from 10 fMRI sessions per subject during rest (eyes open). **B)** This model is then used to generate the neuronal dynamics at a shorter timescale (at milliseconds), which in this work, we quantify using the benchmark FC and brain assemblies framework. **C)**This dynamic measure is then vectorized and fed to a classifier to discriminate between subjects. We apply a cross-validation method that divides the data into train and test sets (repeating 100 times), training on one of the subjects and testing on the remaining sample.

3.2 Results- Searching for the timescale that captures the most distinctive features of intrinsic brain dynamics

We were interested in finding which timescale captures the most distinctive features that underly the human brain's spatiotemporal repertoire. To answer this question, we applied whole-brain computational modelling to recover neurodynamical activity underlying multi-session rs-fMRI data (Zuo et al., 2014) (see description in table 3.1) in association with the brain assemblies framework to extract the spatiotemporal structures in a temporal range from milliseconds to seconds and a machine learning approach implementing a k-nearest neighbors classifier.

Table 3.1: Summary of resting-state dataset (Zuo et al., 2014). In this chapter, we explore at many timescales, the distinctiveness of intrinsic brain dynamics. To examine such a perspective, we analyzed the multi-session rs-fMRI (Zuo et al., 2014); this table contains a short description of such data (see 2.1.1 section of Methods for details)

Dataset	Subjects	Sessions	Duration of each session
Resting-state (Zuo et al., 2014)	30	10 (rest)	10 minutes

3.2.1 Spacetime motifs of different participants across time (10-4000ms)

We calculate the number of spacetime motifs in a range from 10-4000ms, increasing 10ms each time window (binning size). Figure 3.2 shows both the average number of spacetime motifs and its rounding to the next integer in each timescale. In terms of the rounding, the number of features that we use for the classification, we observe that its distribution increases proportionally at increasing time resolution (from 10-100ms) and reaches the maximum in the window of 100-260ms. On the other hand, such distribution decreases inversely to the increasing of time windows size starting from 260ms.

3.2.2 Subject identification

To explore the evolution between milliseconds and seconds of the distinctiveness of whole-brain spacetime motifs, we implemented a classifier based on multinomial logistic regression. More specifically, we calculated the accuracy of both, spatiotemporal structures and FC. Regarding the performance of space-time, this is measured in a binned temporal range from 10-40000ms with increments of 10ms in each timeframe. As shown in figure 3.3, the median accuracy (white dots) to discriminate spatiotemporal assemblies of individual human brains is above 95% across all time scales. While FC, a measure of static correlations from the empirical temporal series, is around 67%.

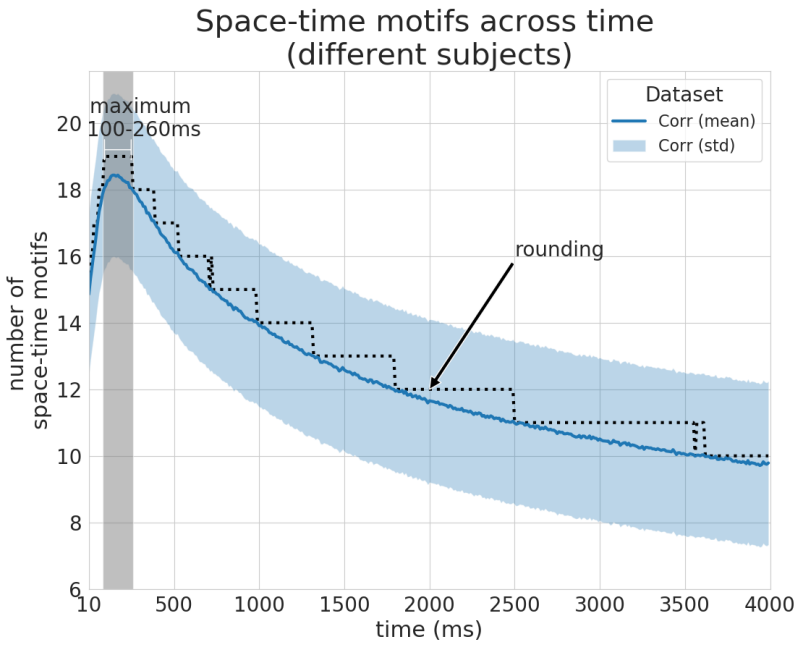

Figure 3.2: Average of spatiotemporal structures across time The mean number of spacetime motifs were calculated at each timescale by averaging the number of eigenvalues above Marčenko–Pastur distribution (Marchenko and Pastur, 1967, Deco et al., 2019) (see chapter 2-Methods). In this graph, we show in blue the mean number of spacetime motifs (y-axis) in a range from 10-4000ms (x-axis). The black dashed line plots the average rounded to the next integer. Grey shading highlights the time window where the maximum number of the spatiotemporal structures was extracted.

.

3.2.3 Contrast of similarity across timescales

The similarity matrices were defined using the PCC between sessions of each participant, in which each element contains the correlation of spatiotemporal features of all participants. In figure 3.4, we display two matrices, both with the relationships between the first and second session of all participants; these matrices confirm that the features that belong to the same participants (values within the diago-

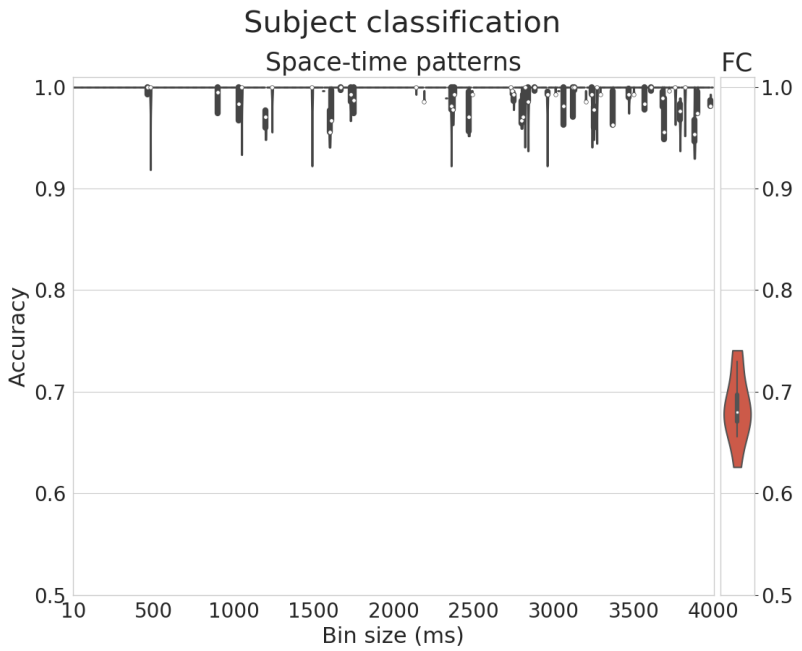

Figure 3.3: Subject classification performance. Classification accuracy comparing the performance of both measures; the dynamic space-time motifs, from 10-4000ms, and the static FC measure. In binned sizes from 10-500ms (higher resolution than the reached using traditional fMRI), the dynamic structures achieve maximal classification accuracy. In contrast, in larger windows (>500ms), such performance decreases but maintains its median above 95% of accuracy. Regarding FC, the median accuracy of the classification is 67%.

nal) are the ones with higher PCC values (warm colors). The values close to 1 on the diagonal confirm the classification performance of the previous section, which demonstrated how the spatiotemporal features accurately discriminate between different participants at different timescales.

Next, for exploring the individuality of the features for each timescale, we measure from the PCC measure, how far away is the second most correlated individual; by calculating, per row, the differ-

ence between the highest and second-highest PCC. We average this difference at each timescale, from 10-4000ms (figure 3.4), and obtain a maximum value of this difference at 190ms and a minimum at 3420ms. For larger differences in similarity, the matrix more clearly contains strong correlations on the diagonal (values 1) and low correlations (close to zero) in the off-diagonal part of the matrix. Figure 7 shows the similarity matrices at the minimum and maximum of the differences (at 190ms and 3420ms, respectively), where both arrangements display that the spacetime patterns discriminates different individuals. Additionally, similarity matrices demonstrate that in a lower temporal resolution, the spatiotemporal features more challenging differentiate participants, as we observe more values close to one (strong relationship) disperse in the matrix.

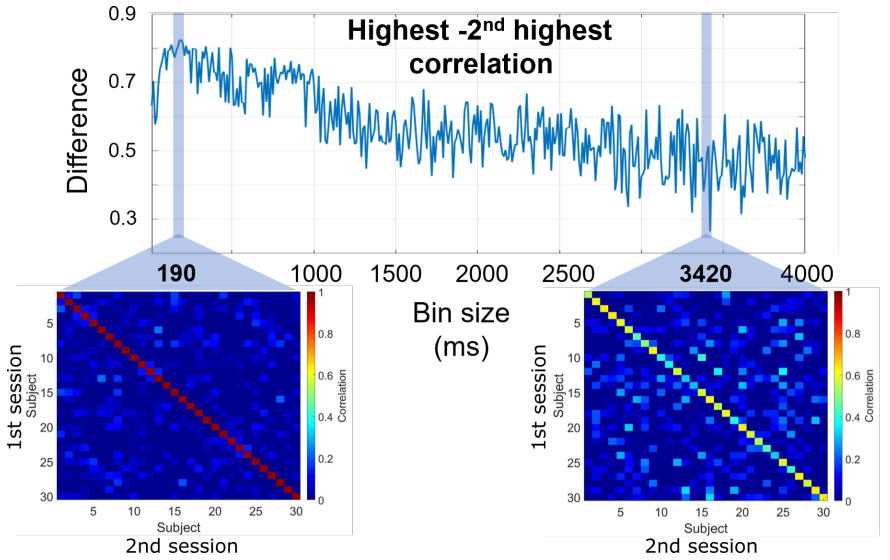

Figure 3.4: Subject similarity, contrast across timescales. Averaged difference between similarity matrices from 10ms-4000ms. The difference reaches its maximum value at 190ms and decreases over time with a minimum at 3420ms. This figure displays the similarity matrices at both boundaries, to observe its contrast; every element contains the PCC between the first and second session of each participant, thus on the diagonal are the values that belong to the same individual. The color scale of the matrices indicates the correlation coefficient between pair of subjects (1 = total correlation and 0 = no correlation), and both matrices evidence perfect subject identification (the warmer values always within the diagonal). However, comparing both arrangements, the matrix at 190ms indicates that features of different individuals (out of diagonal) have a less statistical relationship, showing more values closer to 0 correlation (cold elements in the matrix).

3.3 Discussion

We investigate which is the most relevant time scale for extracting subject-specific brain signature, by the linkage of neuroimaging data with a multiscale computational method. We introduce a multiscale approach that applies whole-brain computational modelling to fMRI data; in which we simulate at milliseconds the synaptic connections

between neurons, based on the structural connectivity of brain regions. Next, we extract individual spatiotemporal patterns of brain activity within the range of 10-4000ms, and finally implement a machine learning classifier to the dynamic patterns, at each timescale. The above enables a better understanding of fundamental brain dynamics and leads to the discovery of personalized medical interventions.

Our results demonstrate that the spatiotemporal structures are so unique among individuals that they can identify, with near-perfect accuracy, a participant from a group. We also show that the individuality of the brain motifs is more delimited at around 200ms, where the structures are much more distinct per-subject. Additionally, similarity among subjects decreases proportionally to the increase of temporal resolution.

The findings of this work are consistent with the previous work of Deco and colleagues that by applying the space-time motifs framework to fMRI data demonstrated that both measures entropy and hierarchy respectively, reach an optimum level at a timescale of approximately 200ms 15. Other studies, that without the application of computational modelling but instead used EEG, found relevant microstates similarly within the same temporal range (200ms) (Koenig et al., 2005; Lehmann et al., 1998). In terms of the research on intrinsic brain dynamics, our results are in line with previous findings that showed the broadcasting of conscious processing at the range of 200–250ms (Del Cul et al., 2007; van Vugt et al., 2018; Dehaene and Changeux, 2011) and provide more insights about at which timescale the human brain encodes spontaneous processes.

In this work, we use fMRI for mapping whole-brain structure and function. However, fMRI has several limitations for studying brain dynamics such as; the indirect nature of this technique (BOLD signals) and its relatively low spatiotemporal resolution, which is on the scale of seconds (Logothetis, 2008). For studying the most specific spatiotemporal domain of brain dynamics, we propose our multiscale approach. We overcome fMRI limitations, by applying whole-brain modelling that based on anatomical connections recovers neuronal dynamics at milliseconds (Deco et al., 2014). This model combined with the extraction of spatiotemporal motifs that through binned temporal windows, tracks dynamic patterns of brain activity at may timescales (Deco et al., 2019). Our approach is different from existing measures, first because of its flexibility to study the human brain at different timescales. Additionally, due to the dynamic nature of the space-time features, our method tracks spatiotemporal patterns of brain activity that compared with benchmark measures are based on static measures.

Whole-brain computational modeling has played an important role for understanding intrinsic brain dynamics (Cabral et al., 2014), and neuropsychiatric disorders (Deco and Kringelbach, 2014). On the other hand, computational models combined with the extraction of spatiotemporal features could thus play a significant role not only for a better understanding of intrinsic brain dynamics 15, but also opens up to get a personalized care of neurological disruptions (Falcon, Jirsa, et al., 2016). Besides, subject-based perspective may improve some treatments by predicting the outcome, but also more generally in the discovery of biomarkers. In general terms, the application of

brain modeling for an individualized medicine have demonstrated a high relevance for clinical interventions of epileptic patients 11 and stroke recovery (Falcon, Riley, et al., 2016).

In summary, computational methods, such as whole-brain modelling (Deco and Kringelbach, 2014; Deco et al., 2008) and machine learning (Vu et al., 2018), complement traditional neuroimaging techniques to study brain dynamics at different timescales. However, future work is needed to study brain dynamics while performing cognitive processes and possible disruptions of such dynamics in clinical population. Overall, we believe our work opens future benefits to base medical practices on the individual characteristics of patients (Vogenberg et al., 2010), as well as for predicting the course of neuropsychiatric disorders (Ozomaro et al., 2013).

Chapter 4

Study 2: Spatiotemporal domain of task-based cognition

4.1 Introduction

Contemporary views of whole-brain dynamics propose that human brain functions emerge from embedded dynamics of integrated neural elements that operate as a whole (Deco and Kringelbach, 2017; Huys et al., 2014; Perdikis et al., 2011). The characterization at many timescales of neural functions introduced novel computational theories of healthy information processing in behavior (Perdikis et al., 2011) as in cognition (Woodman et al., 2011). In this line, recent timescale characterization studies established that pathological conditions, like epilepsy, are associated with disturbances in the brain dynamics (V. K. Jirsa et al., 2014). The above could be reflected, for example, in neuropsychiatric patients' core symptoms, such as

in visual hallucinations and thought disorder common symptoms in schizophrenia (Spencer et al., 2004).

Recent multimodal brain imaging research has established that whole-brain dynamics contain signatures of specific cognitive states Michels et al., 2010. Furthermore, a study that simultaneously used magnetic resonance imaging (MR), positron emission tomography and electroencephalography, found that it is possible to identify subjects based on their resting-state activity alone alone (Shah et al., 2017). This ability to decode any condition- or subject-specific information from measured brain activity is a strong indication that we can identify both trait and state-dependent features of neural processing.

By combining multiple brain imaging techniques, it possible to reach a more extensive spatiotemporal domain than using a single method, due to none of the existing neuroimaging techniques can capture brain activity on both a broad spatial and temporal scale simultaneously. However, it is still not well understood at which spatiotemporal scale the brain operates when performing a task, and multimodal approaches are costly and prone to artefacts (Steyrl et al., 2015).

To overcome the experimental difficulties of measuring brain signals with a single technique, a computational whole-brain model can be used to supplement signals in the inaccessible spatiotemporal range. In previous work, Deco and colleagues proposed a novel framework to extract whole-brain features named “space-time motifs” (Deco et al., 2019); these motifs are spatiotemporal and dynamical structures across the brain. The proposed framework aims at identifying groups

of brain regions with co-activation patterns and tracking this activity at many timescales by applying a computational model.

In this study, we use machine learning (as shown in fig4.1) to uncover the most distinctive spatiotemporal domain of brain dynamics from a classification perspective. First, we apply a computational whole-brain model, that recovers neural signals from fMRI data at the millisecond timescale (Deco et al., 2014), and the "Brain assemblies" method across temporal scales (Deco et al., 2019), which extracts the co-activation patterns of brain regions from milliseconds to seconds. After that, we implement aclassifier based on multinomial logistic regression (MLR) to separate different conditions. In our approach, we classify the dynamic spatiotemporal structures in comparison with benchmark methods such as functional connectivity (FC) (which calculates whole-brain activity based on static spatial correlations) and evaluate which is the most distinctive spatiotemporal domain to classify cognitive conditions.

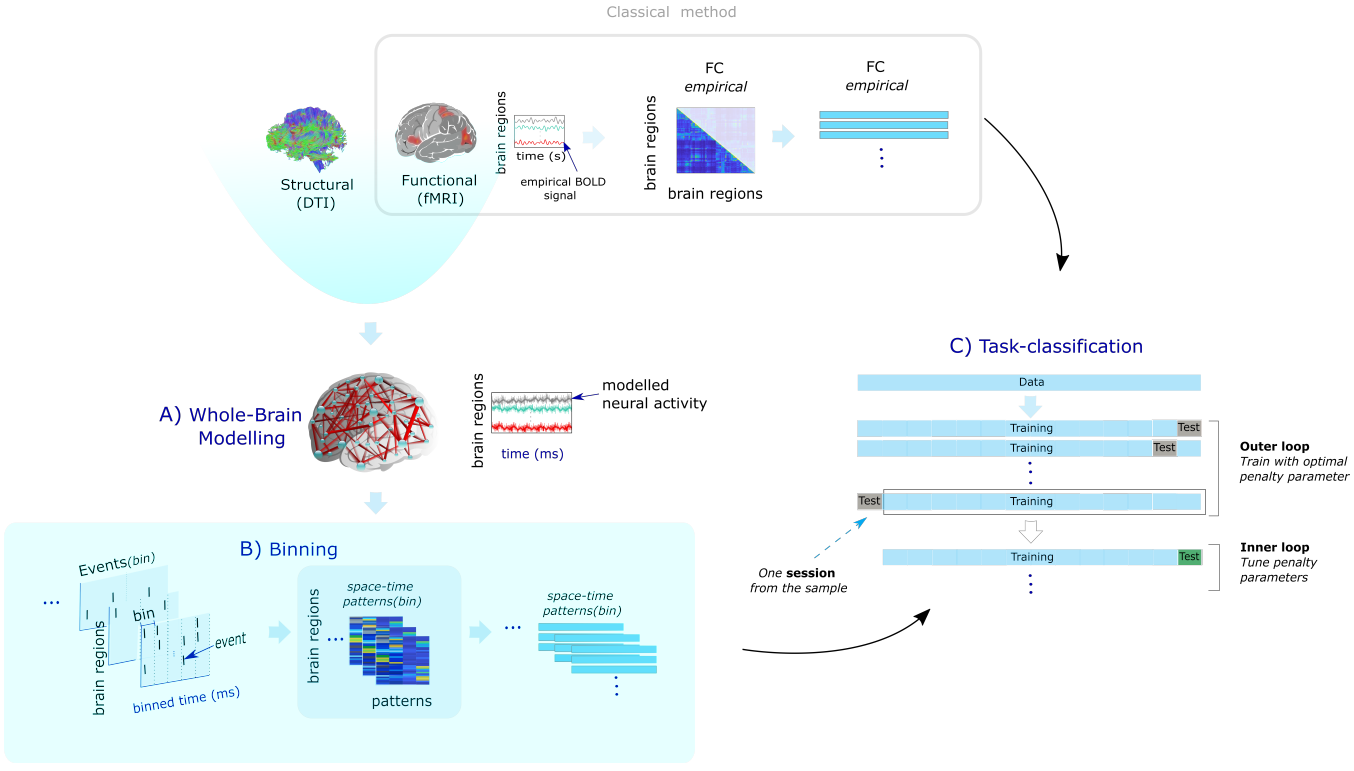

Figure 4.1: Workflow for the classification of cognitive-based tasks. The methodology of this study can be summarized as follows; the implementation of **A)** Whole-brain modelling of BOLD signals, to recover the intrinsic neurodynamical time-series (in milliseconds). Followed by the **B)** Binning of the modelled output, where time windows are created from milliseconds to seconds, in order to extract the spacetime motifs(bin) at many timescales. Lastly, the implementation across binned timeframes of the MLR **C)** classifier to the vectorized FC and brain assemblies measures, for capturing the distinctiveness of each cognitive task over time.

4.2 Results- Spatiotemporal domain that captures the most characteristic features of brain cognition

As a second study, we apply our multiscale method for classifying different tasks. We are particularly interested in examining which range of timescales extracts the most particular features of human cognition. We apply whole-brain modelling to the task-related dataset Senden et al., 2017 (see a summary in table 4.1 or 2.1.2 section for details) to recover neurodynamical activity, and the brain songs framework to extract the spatiotemporal structures from milliseconds to seconds. Moreover, we use the multinomial logistic regression and k-nearest-neighbor classifiers to separate between conditions across timescales.

4.2.1 Space-time motifs of cognitive tasks across time (10-4000ms)

In this section, we calculate the spatiotemporal activity patterns of different cognitive tasks motifs, from 10-4000ms and a binning size of 10ms (figure 4.2). We observe in figure 9 the average number of the dynamical structures as well as its rounding (to the nearest larger integer). As in the previous chapter, we use the rounding as a guide for extracting this number of co-activation patterns (see methods). Notice that the number of activity patterns increases proportionally from 10-90ms, reaches its maximum at the range of 90-260ms, and

Table 4.1: Summary of task-related dataset from Senden et al., 2017. As a second study of this manuscript, we analyze at the range of 10-4000ms, what is the most the particular timescale for separating cognitive tasks. To that end, we analyze the task-related dataset Senden et al., 2017, which short description is in this table (see 2.1.2 section of Methods for specific information)

Dataset	Subjects	Sessions (each participant)	Duration
Task-related Senden et al., 2017	14	1 resting-state	8 minutes
		1 n-back taskKirchner, 1958	$\sim$ 7 minutes
		1 mental rotation taskShepard and Metzler, 1971	$\sim$ 7 minutes
		1 mental flanker taskEriksen and Eriksen, 1974	$\sim$ 7 minutes
		1 odd-man-outFlowers and Robertson, 1985	$\sim$ 7 minutes

starts to decrease at coarser resolutions (from 260ms).

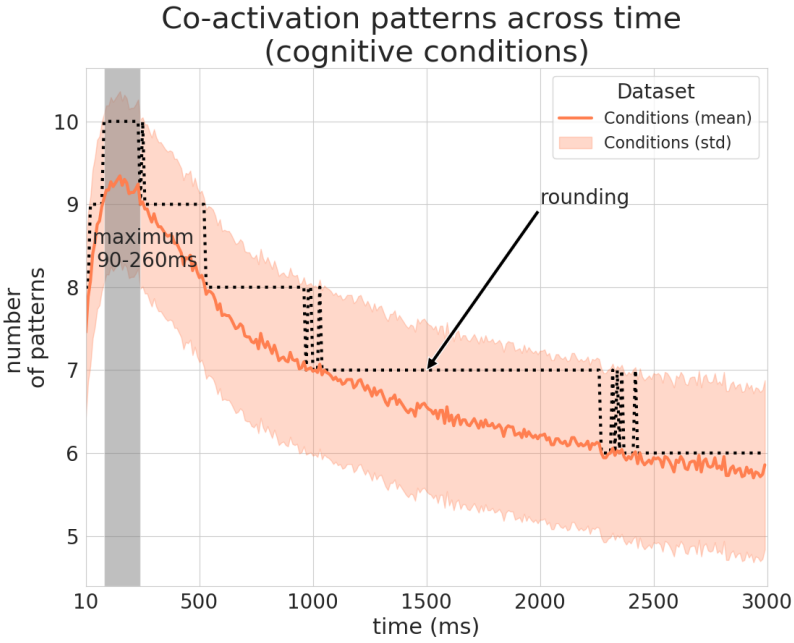

Figure 4.2: Average of spatiotemporal structures across time. Here we display, from 10-4000ms, the average number of space-time motifs of the task-related dataset. We estimate this number counting the eigenvalues above Marčenko–Pastur distribution (Lopes-dos-Santos et al., 2013; Deco et al., 2019) (see section 2.5.1). This graphic plot the mean number of space-time motifs (y-axis) at each time window (x-axis), for all sessions corresponding to different conditions (orange color). Black dashed line traces the rounding to the next integer. Regarding the grey shading, it highlights the range of timescales with the maximum number of the spatiotemporal structures.

4.2.2 Spatiotemporal distinctiveness cognitive function related

For studying the distinctiveness of cognitive tasks and its evolution from milliseconds and seconds, we implemented the classification

from 10-40000ms. We calculated the accuracy of both space-time motifs (from 10-40000ms) and FC. As shown in figure 4.3, the median accuracy (white dots) of classification performance using empirical FC is 80%. On the other hand, the performance of classifying the space-time patterns, that is measured in binned windows with increments of 10ms, accurately discriminate between tasks in higher resolutions (<70ms) and become noisy when increasing the timescale.

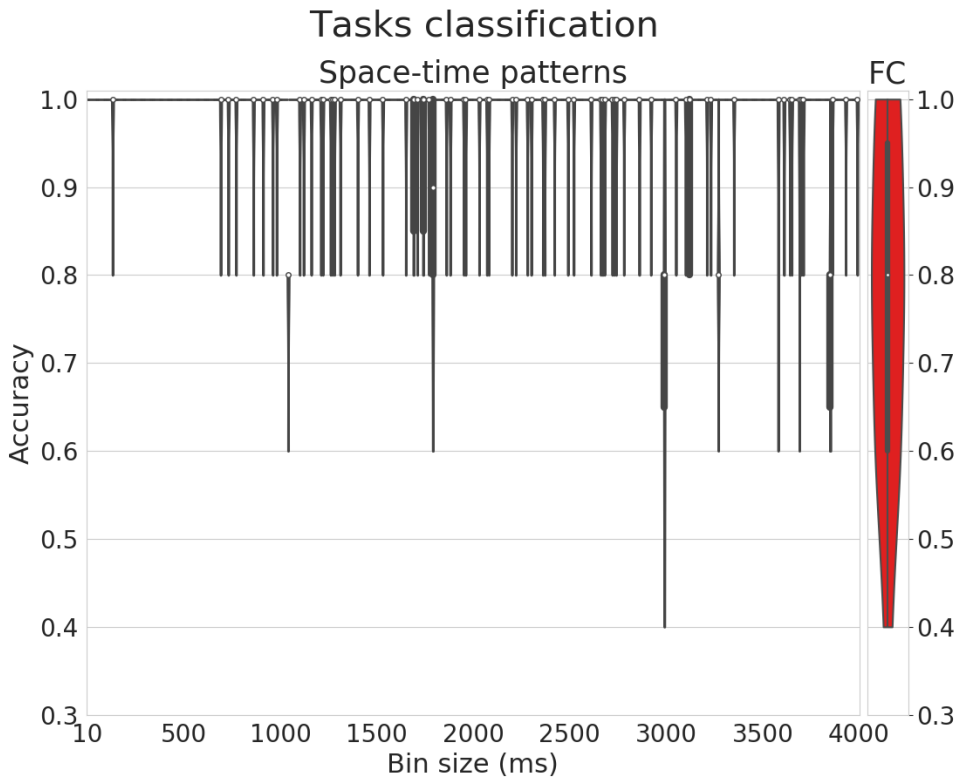

Figure 4.3: Classification performance of brain assemblies from 10-4000ms in comparison with FC. From 10-700ms, a higher temporal domain than the reached using traditional fMRI, the classification using the spatiotemporal patterns achieve 100% of accuracy. In contrast, in larger windows (>700ms), such performance decreases but maintains its median at least 80% of accuracy. Regarding FC, the median accuracy of the classification is 80%.

4.2.3 Spatiotemporal similarity contrast cognitive function related

In addition to the classification, we evaluate the distinctiveness of different tasks across timescales. To achieve this, we calculate per row of the similarity arrangements, the difference between the highest and second-highest PCC (see methods). In figure 4.4, we plot the average of this difference from 10-4000ms; its maximum value is at 150ms and its minimum at 3000ms, respectively. We display similarity matrices at previously mentioned limits; the PCC values separate different tasks (PCC values 1 whiting the diagonal) at 150ms, while at 3000ms there are more intermediate values disperse in the matrix. It is important to remark that the particularity of the conditions starts to decrease after reaching 190ms (maximum limit) and becomes noisier at lower resolutions (approximately at windows higher than 500ms).

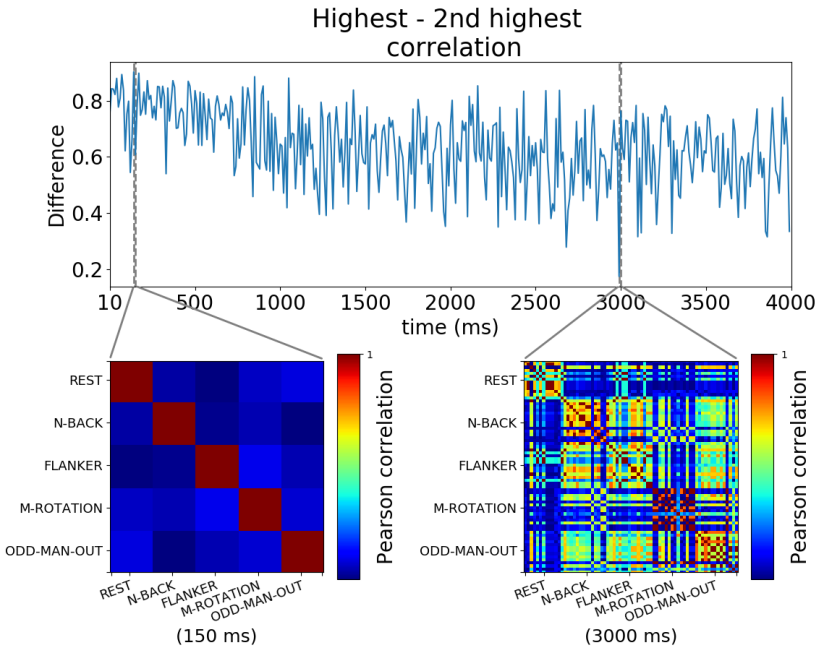

Figure 4.4: Similarity between participants of cognitive tasks, contrast across timescales. Heat map indicates PCC values between pairs of subjects (1 = total correlation and 0 = no correlation). The solid line (in blue) denotes the mean difference between similarity matrices from 10ms-4000ms. Such difference reaches its maximum value at 150ms and decreases over time with a minimum at 3000ms. We display similarity matrices at both maximum and minimum bounds of the averaged difference; Notice that both matrices accurately separate different conditions (higher values in the diagonal), however, the similarity within tasks is higher at 150ms than at 3000ms.

4.3 Discussion

In this study, we investigated a central question in cognitive science, namely if there is a more relevant range of timescales for processing cognitive tasks, which is the most characteristic range. For example, which is the most characteristic range of timescales, for the organization in time in broadcasting information available across the whole-brain, this considering information as the encoding of cognitive tasks.

As the general workflow 4.1 shows (for details, see chapter 2), we apply the brain assemblies' approach from Deco et al., 2019 from a classification perspective across timescales. We first A) fit a whole-brain dynamic mean-field (DMF) model (Deco et al., 2014) with pools of excitatory and inhibitory neurons as well as synaptic dynamics to BOLD fMRI data and generate time-series on the timescale of milliseconds. Secondly, we bin this data on different time windows in a range from milliseconds to seconds (10ms-4000ms), and for each of these windows, we extract the brain assemblies to characterize the dynamical repertoire of the whole-brain. C) And finally, we apply a classifier, across timescales, to the brain assemblies and FC measures to separate from fMRI dynamics different cognitive tasks; We specifically analyze fMRI data of healthy controls that include both rs-fMRI as well as tasks such as; mental rotation (Shepard and Metzler, 1971), odd-man-out (Flowers and Robertson, 1985), flanker (Eriksen and Eriksen, 1974) and n-back (Kirchner, 1958) tasks. See a summary of the task-related dataset (Senden et al., 2017) in the table 4.1 and a detailed description in section 2.1.2).

Our findings suggest that the spatiotemporal motifs characterize, with

almost perfect accuracy, whole-brain dynamics of processing cognitive tasks. In detail, we apply our classification approach based on a multinomial logistic regression to the traditional FC and the novel brain assemblies' measures, classifying the spatiotemporal structures from 10-4000ms. The classification performance demonstrates that in a range ∼10-700ms (at milliseconds) the spatiotemporal nature of the brain assemblies perfectly discriminate different cognitive states whereas the median accuracy of the static FC is 80% (4.3). Moreover, from the co-activation patterns, we contrast the similarity between subjects across timescales; which demonstrates that 150ms is the most characteristic timescale to differentiate between conditions (4.4). It is important to remark, that the millisecond's scale is not accessible using only fMRI, in this study, we access to milliseconds applying the DMF model that incorporates neuronal dynamics (Deco et al., 2014; Deco et al., 2019) together with binned time windows to access a broader domain from milliseconds to seconds (see methods in section 2.4.1).

As we show in our study, the relevant timescale for characterizing both resting and tasks is not in the order of seconds but rather faster closer to 200ms which is consistent with previous findings on MEG and fMRI data (Deco et al., 2019). Our findings are in concordance with the previous work of Deco and colleagues that by applying the space-time motifs framework to fMRI data demonstrated that both, measures of entropy as well as a hierarchy, reach an optimum level at a timescale of approximately 200ms (Deco et al., 2019). Other studies, that without the application of computational modeling but instead used EEG, found relevant microstates similarly within the

same temporal range (∼200ms) (Koenig et al., 2005; Lehmann et al., 1998). More recent studies found a functional signature of brain networks using task-related fMRI datasets (**jung2018**).

Concerning our outcome for separating cognitive tasks, it indicates that precisely at 150ms is the most characteristic timescale, in this context, a previous study showed that infant facial features evoke activity in the orbitofrontal cortex within 130ms (M. L. Kringelbach et al., 2008). The above could be related to fast processes across temporal hierarchies related to human cognition (M. L. Kringelbach et al., 2015).

The consistency in the range of timescales (∼200ms) across both resting and tasks experimental conditions suggests that it might be an intrinsic property of brain dynamics. Nevertheless, the exact relationship between the temporal organization and brain processing remains unclear.

In summary, computational methods, such as whole-brain modelling (Deco and Kringelbach, 2014; Deco et al., 2008) and machine learning (Vu et al., 2018), complement traditional neuroimaging techniques to study brain dynamics at different timescales. However, future research is needed for investigating this temporal organization with a multiscale approach that effectively characterizes neural dynamics of the information processing in both behavior and cognition as well as their possible disruptions such as in the case of neuropsychiatric disorders.

Chapter 5

Study 3: Timescale characterization study of neuropsychiatric disorders

We dedicate this chapter for studying the intrinsic dynamics of human brain, in both healthy individuals and participants with neuropsychiatric syndromes. We specifically study disorders such as schizophrenia, bipolar disorder, and attention deficit/hyperactivity disorder ADHD. In this study, we apply our multiscale approach spanning timescales from milliseconds to seconds in order to identify the timescale that better discriminates neuropsychiatric conditions (see in fig.5.1, a summary of the pipeline).

5.1 Introduction

Brain dynamics has shown a high neural organization for processing complex functions, also known as cognitive coordination. This coordination of neural elements is apparently organized in a dynamic and broad domain that comprises both space and time. One of the hypotheses for explaining such an organization establishes that it is given by a set of neural processes that control the timing of spiking among cells (W. A. Phillips and Silverstein, 2003; J. Phillips et al., 2012).

The development of new experimental methodologies for studying the whole brain such as computational modeling, has contributed to establishing more hypotheses of the organization of healthy brain dynamics, how it works even during rest (Deco, Kringelbach, et al., 2017; Deco et al., 2013), and at processing complex functions (Deco et al., 2019). This knowledge of healthy mechanisms may work as a base for studying possible disruption in neuropsychiatric disorders' dynamics.

Current approaches for studying neuropsychiatric disorders emphasize the possible relationship between neuronal disorganization and neuropsychiatric conditions. For instance, this neuronal discoordination has been identified in schizophrenia (Krajcovic et al., 2019; Spencer et al., 2004). The neural coordination hypothesis based on functional groups of neurons called cell assemblies (Hebb, 1949 (see *Neuronal assemblies*) could be affected in such a way that disturbs neuron activity timing. A recent work that studied psychosis demonstrated such disbalance reflected in a cognitive disorganization

(Olypher et al., 2006).

We aim to study how brain dynamics are affected in neurocognitive domains by applying computational whole-brain modeling and brain assemblies theory. We use machine learning (pipeline shown in fig 5.1, see Chapter 2 for details) to uncover the most distinctive spatiotemporal domain of brain dynamics from a classification perspective (of both healthy and patient groups). First, we apply a computational whole-brain model that recovers neural signals from fMRI data at the millisecond timescale (Deco et al., 2014) and the "Brain assemblies" method across temporal scales (Deco et al., 2019), which extracts the co-activation patterns of brain regions from milliseconds to seconds. After that, a multinomial logistic regression (MLR) classifier to separate different conditions. In our approach, we classify the dynamic spatiotemporal structures compared with benchmark methods such as functional connectivity (FC) (which calculates whole-brain activity based on static spatial correlations) and evaluate which is the most distinctive spatiotemporal domain to classify cognitive conditions.

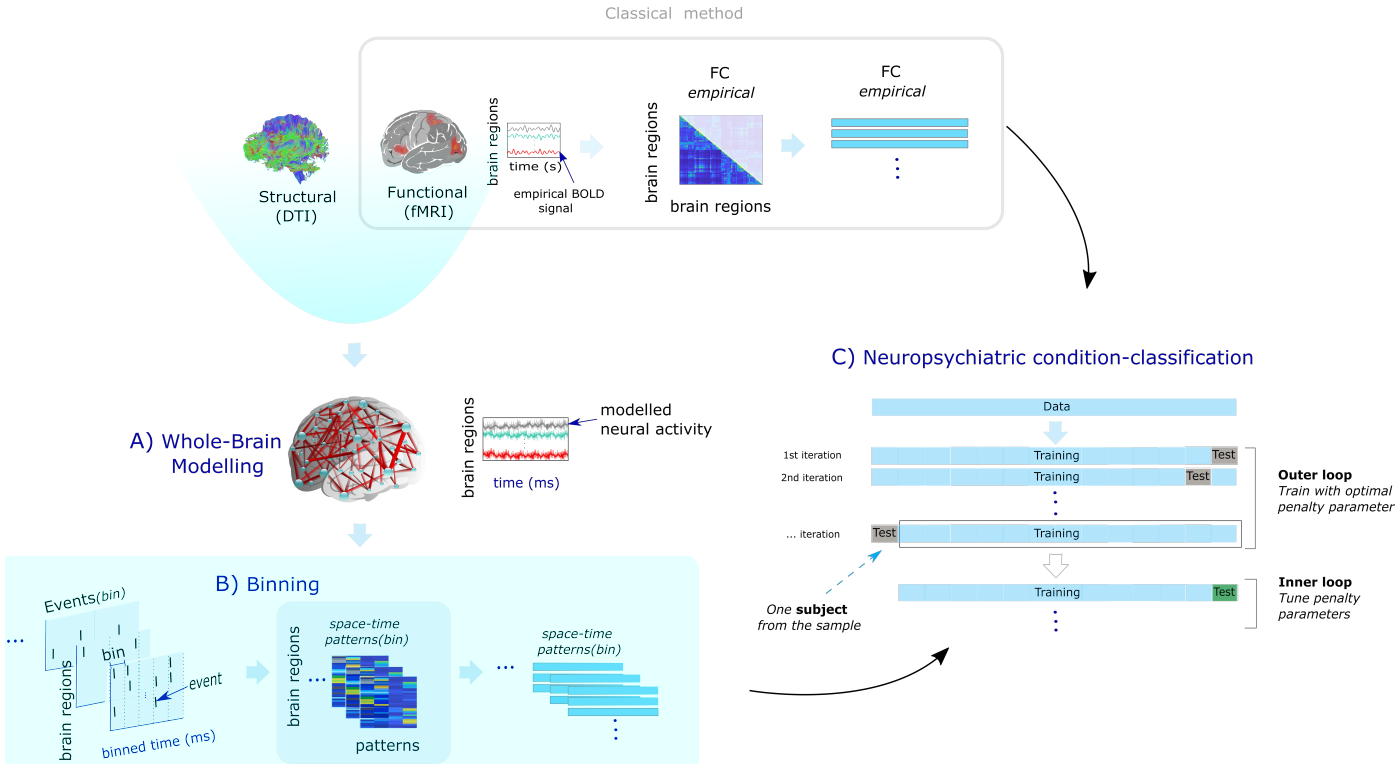

Figure 5.1: Methodology for separating neuropsychiatric conditions. To calculate across timescales the classification of neuropsychiatric conditions, firstly, we apply **A)** Whole-brain modelling of BOLD signals, to recover the intrinsic neurodynamical time-series (in milliseconds). Followed by the **B)** Binning of the modelled output, where time windows are created from milliseconds to seconds, in order to extract the spacetime motifs(bin) at many timescales. Lastly, the implementation across binned timeframes of the **C)** classifier to the space-time motifs(bin), for capturing the particularity of each neuropsychiatric condition across time.

5.2 Results- Tracking the most important timescale to differentiate brain disorders

5.2.1 Spatiotemporal patterns of brain activity of neuropsychiatric conditions (10-4000ms)

This section is dedicated to the application of our multiscale approach to classify, from patterns of brain activity, different cognitive conditions. We first extract the average number of space-time motifs from 10-4000ms. As shown in figure 5.2, the space-time motifs increase their number in low resolutions (milliseconds scale) and reach its maximum at the range of 80-310ms. From 310ms, the average number of the spatiotemporal structures decreases proportionally to the timescale increment.

5.2.2 Spatiotemporal distinctiveness of neuropsychiatric disorders

We evaluate the distinctiveness, across timescales, rs-fMRI of both healthy and neuropsychiatric states. To achieve this, we calculate the difference between the highest and second-highest PCC (details in the methods section) of between-subjects similarity matrices. In figure 5.3, we show the average of this difference from 10-4000ms; with its maximum at 420ms and its minimum at 2540ms, respectively.

Table 5.1: Summary of neuropsychiatric conditions dataset (Poldrack et al., 2016). We dedicate this chapter for studying across timescales (10-4000ms) the brain dynamics signature of different cognitive disorders. We explicitly study the neuropsychiatric fMRI datasetPoldrack et al., 2016; this dataset contains data from both healthy controls and from different neuropsychiatric conditions such as schizophrenia, ADHD and bipolar disorder. This table contains a brief description of such dataset, for more details see the 2.1.3section of Methods.

Dataset	One session (each participant)	Subjects (256)	Conditions
Neuropsychiatric condition Poldrack et al., 2016	rs-fMRI (304s)	130	Healthy controls
		50	Schizophrenia
		43	ADHD
		49	Bipolar disorder

The distinctiveness of the conditions starts to decrease after reaching 420ms (maximum limit of mean difference) and becomes noisier at lower resolutions (approximately at timescales higher than 500ms). We observe that the PCC values separate neuropsychiatric disorders at 420ms (maximum mean difference). In comparison, at 2540ms (minimum limit of mean difference) there are lower correlations values in the diagonal, but also high PCC values between different conditions; such in the case of correlations between healthy controls and ADHD.

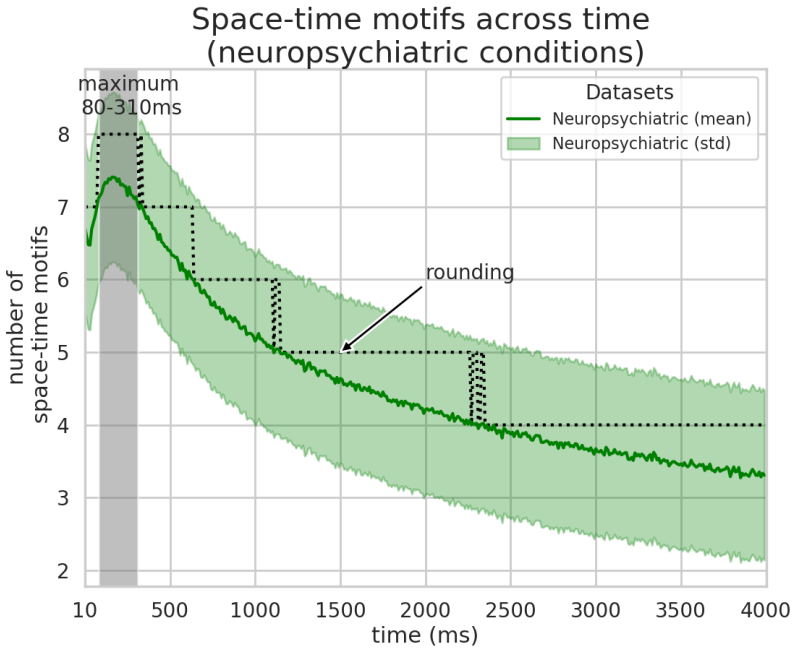

Figure 5.2: Average of spatiotemporal structures across time The average number of co-activation patterns (from 10-4000ms, x-axis) of the dataset that comprises neuropsychiatric illness (in green); black dashed line represents the rounded averaged. This number reaches its maximal in the range of 80-310ms (grey shading of the graph), and after reaching this maximum, the number of space-time motifs decreases at lower temporal resolutions.

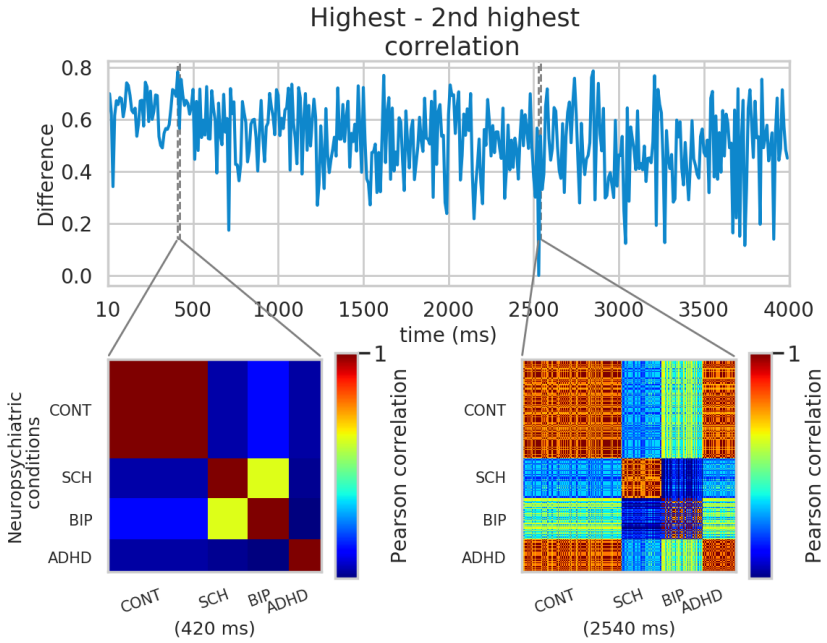

Figure 5.3: The similarity between participants, and contrast across timescales of healthy and neuropsychiatric conditions Mean difference between similarity matrices from 10ms-4000ms in blue. The difference reaches its maximum at 420ms and decreases over time with a minimum at 2540ms. We display similarity matrices at both maximum and minimum bounds of the averaged difference; Heat map indicates PCC values between pair of participants (1 = total correlation and 0 = no correlation). Axes of similarity matrices indicate the label of each condition (Abbreviations: CONT, healthy participants; SCH, schizophrenia; BIP, bipolar disorder; ADHD, Attention Deficit Hyperactivity Disorder). At 420ms, the similarity matrix accurately differentiates all conditions.

5.3 Discussion

This study focuses on extracting informative spatio-temporal features from fMRI dynamics of healthy individuals and individuals with neuropsychiatric disorders from Poldrack et al., 2016. Our approach incorporates a model-based characterization of time scales, aiming to find the most informative timescale for separating from brain dynamics neuropsychiatric conditions.

As the general methodology that figure 5.1 describes (for details, see methods in chapter 2), we apply the brain assemblies' approach (Deco et al., 2019) from a classification perspective across timescales. We first A) fit a whole-brain dynamic mean-field (DMF) model that incorporates pools of excitatory and inhibitory neurons and synaptic dynamics to BOLD fMRI data and generate time-series on the timescale of milliseconds (Deco et al., 2014). Secondly, we bin this data on different time windows in a range from 10ms-4000ms, and for each of these windows, we extract the brain assemblies to characterize the dynamical repertoire of the whole-brain. C) Finally, we apply a classifier based on multinomial logistic regression, in the temporal domain from milliseconds to seconds (10ms-4000ms), to the brain assemblies and FC measures to separate from fMRI dynamics different neuropsychiatric conditions. We specifically analyze rs-fMRI data of both healthy and patient groups. Patients' data incorporates schizophrenia, bipolar disorder, and attention-deficit/hyperactivity disorder. See a summary of the neuropsychiatric conditions' dataset (Poldrack et al., 2016) in table 5.1 and more details in section 2.1.3.

Our findings suggest that the space-time motifs characterize, with

almost perfect accuracy, whole-brain dynamics of neuropsychiatric conditions (see section 5.2.2). In detail, we apply our classification approach based on a multinomial logistic regression (MLR) to the traditional FC and the novel brain assemblies' measures as figure 5.1.C shows. We explicitly classify, from 10-4000ms, using the spatiotemporal structures and FC as input. The classification performance demonstrates that the dynamics nature of the brain assemblies perfectly discriminates different cognitive states. Moreover, from the co-activation patterns, we contrast the similarity between subjects across timescales; which demonstrates that $\sim$420ms is the most characteristic timescale to differentiate between conditions. It is important to remark, that the millisecond's scale is not accessible using only fMRI, in this study, we access to milliseconds applying the DMF model that incorporates neuronal dynamics (Deco et al., 2014) together with binned time windows to access a broader domain from milliseconds to seconds (see section 2.4.1).

Our findings suggests a temporal disruption of intrinsic intrinsic brain dynamics. Our timescale characterization for separating neuropsychiatric disorders shows an optimal distinctiveness at $\sim$400ms, a longer timescale than the range found in previous work that analized healthy rs-fMRI Deco et al., 2019. Our results indicates that neuropsychiatric conditions may have bases on spatiotemporal alterations of brain dynamics. Previous studies of mental disorders (Fonov et al., 2009) supported such hypothesis and demonstrated disturbances in spatial- temporal mechanism (Dawson, 2004 such as schizophrenia (Northoff et al., 2020) and autism spectrum disorders (Wass, 2011), (Watanabe et al., 2019). Indeed the severity of

some symptoms of autism has been associated with a longer intrinsic timescale of particular brain areas (Watanabe et al., 2019). In this line, the recently introduced concept of 'Spatiotemporal Psychopathology' also suggests the relevance of taking into consideration possible disruptions of both the spatial and temporal domain in psychiatric disorders (Northoff, 2016; Northoff, 2018; Northoff, 2018). Future studies are needed to examine this possible disbalance in space and time of neuropsychiatric brain dynamics. Such a hypothesis might be further studied by extracting patterns of interacting neuronal assemblies (Fingelkurts and Fingelkurts, 2019; Deco et al., 2019).

Brain dynamics shows a complex organization at many spatiotemporal scales (Deco et al., 2011; Perdikis et al., 2011), a proper characterization of temporal scales could provide some guidance for experimental steps. Whole-brain computational modeling has played an important role for understanding intrinsic brain dynamics (Cabral et al., 2014), and neuropsychiatric disorders (Deco and Kringelbach, 2014). On the other hand, computational models combined with the extraction of spatiotemporal features could thus play a significant role not only for a better understanding of intrinsic brain dynamics (Deco et al., 2019) , but also opens up to get a personalized care of neuropsychiatric disruptions (Falcon, Jirsa, et al., 2016). Besides, subject-based perspective may improve some treatments by predicting the outcome, but also more generally in the discovery of biomarkers. In general terms, the application of brain modeling for an individualized medicine have demonstrated a high relevance for clinical interventions of epileptic patients (V. K. Jirsa et al., 2017) and stroke

recovery (Falcon, Riley, et al., 2016).

In summary, computational methods, such as whole-brain modelling (Deco and Kringelbach, 2014; Deco et al., 2008) and machine learning (Vu et al., 2018), complement traditional neuroimaging techniques to study brain dynamics at different timescales. However, future work is needed to study brain dynamics while performing cognitive processes and possible disruptions of such dynamics in clinical population. Overall, we believe our work opens future benefits to base medical practices on the individual characteristics of patients (Vogenberg et al., 2010), as well as for predicting the course of neuropsychiatric disorders (Ozomaro et al., 2013).

Chapter 6

General discussion

In this work, we applied a multiscale method for extracting the most informative time scale of human brain dynamics from three different decoding schemes: to separate different participants, cognitive tasks, and neuropsychiatric conditions; we describe such perspectives as separated studies, according to the analysis of fMRI data, i.e., resting-state data (Zuo et al., 2014), task-based dataset (Senden et al., 2017), and neuropsychiatric conditions (Poldrack et al., 2016), respectively. We summarize our multiscale methodological approach in three main steps; first, we fit a whole-brain model of BOLD signals to recover the intrinsic neurodynamical time-series (in milliseconds). Secondly, we apply the modeled output's binning, where time windows are created from milliseconds to seconds to extract the spatiotemporal motifs(bin) at many timescales. Lastly, the implementation across binned timeframes of the classifier to the spacetime motifs(bin) captures each condition's particularity (different individuals, tasks, and neuropsychiatric disorders) across time.

6.1 Relevance of multiscale approaches in experimental neuroscience

Recent theories of brain information processing point out the importance of characterizing brain dynamics at multiple timescales (Perdikis et al., 2011), these analysis have become increasingly important for studying baseline dynamics (Morcom and Fletcher, 2007), cognitive processes (M. L. Kringelbach et al., 2015) and brain disorders (Lytton et al., 2017; V. K. Jirsa et al., 2014; Fingelkurts and Fingelkurts, 2019).

We introduce a multiscale approach that applies whole-brain computational modelling to fMRI data; in which we simulate the synaptic interactions between neurons at the milliseconds timescale, based on the structural connectivity of brain regions. Next, we extract spatiotemporal patterns of brain activity across the range of 10-4000ms and apply a machine learning classifier to the dynamic patterns, for each timescale. We focus on three different classes: subjects, cognitive tasks and neuropsychiatric disorders. For each of these classes, we aim to identify the most relevant time scale for extracting the brain signature. The above enables a better understanding of fundamental brain dynamics and leads to the discovery of personalized medical interventions.

Our results demonstrate that the spatiotemporal structures are so unique among individuals that they can help to identify, with near-perfect accuracy, a condition from a set. Additionally, similarity among patterns of activity decreases proportionally to the increase

of temporal resolution. More importantly, the distinctiveness of these space-time motifs is maximized at timescales that are not reached by using only fMRI.

Regarding both resting-state and tasks, the most characteristic timescale is around 200ms, where the brain assemblies are much more distinct. Our findings regarding intrinsic brain dynamics are consistent with the previous work of Deco and colleagues that by applying the space-time motifs framework to fMRI data demonstrated that both, measures of entropy as well as hierarchy, reach an optimum level at a timescale of approximately 200ms (Deco et al., 2019). Other studies, that without the application of computational modelling but instead used EEG, found relevant microstates similarly within the same temporal range (200ms) (Koenig et al., 2005; Lehmann et al., 1998). In terms of the research on intrinsic brain dynamics, our results are in line with previous findings that showed the broadcasting of conscious processing at the range of 200–250ms (Del Cul et al., 2007; van Vugt et al., 2018; Dehaene and Changeux, 2011), and provide more insights about at which timescale the human brain encodes spontaneous processes.

Concerning our outcome for separating cognitive tasks, it indicates that precisely at 150ms is the most characteristic timescale, in this context, a previous study showed that infant facial features evoke activity in the orbitofrontal cortex within 130ms (M. L. Kringelbach et al., 2008). The above could be related to fast processes across temporal hierarchies related to human cognition (M. L. Kringelbach et al., 2015).

In contrast with our analyzes of healthy participants, the timescale for discriminating neuropsychiatric conditions suggests a disruption of intrinsic dynamics. Neuropsychiatric disorders showed an optimal distinctiveness at a longer timescale (400ms). This result indicates that neuropsychiatric conditions may have bases on spatiotemporal alterations of brain dynamics. Previous studies of mental disorders (Fonov et al., 2009) supported such hypothesis and demonstrated disturbances in spatial- temporal mechanism (Dawson, 2004 such as schizophrenia (Northoff et al., 2020) and autism spectrum disorders (Wass, 2011), (Watanabe et al., 2019). Indeed the severity of some symptoms of autism has been associated with a longer intrinsic timescale of particular brain areas (Watanabe et al., 2019). In this line, the recently introduced concept of 'Spatiotemporal Psychopathology' also suggests the relevance of taking into consideration possible disruptions of both the spatial and temporal domain in psychiatric disorders (Northoff, 2016; Northoff, 2018; Northoff, 2018). Future studies are needed to examine this possible disbalance in space and time of neuropsychiatric brain dynamics. Such a hypothesis might be further studied by extracting patterns of interacting neuronal assemblies (Fingelkurts and Fingelkurts, 2019; Deco et al., 2019).

6.2 Potentials and pitfalls of the different models

In this work, we use fMRI for mapping whole-brain structure and function. However, fMRI has several limitations for studying brain dynamics such as; the indirect nature of this technique (BOLD signals) and its relatively low temporal resolution, which is on the scale of seconds (Logothetis, 2008). For studying the most specific spatiotemporal domain of brain dynamics, we propose our multiscale approach. We overcome fMRI limitations, by applying whole-brain modelling that based on anatomical connections recovers neuronal dynamics at milliseconds (Deco et al., 2014). This model combined with the extraction of spatiotemporal motifs that through binned temporal windows, tracks dynamic patterns of brain activity at may timescales (Deco et al., 2019). Our approach is different from existing measures, first because of its flexibility to study the human brain at different timescales. Additionally, due to the dynamic nature of the space-time features, our method tracks spatiotemporal patterns of brain activity that compared with benchmark measures are based on static measures.

6.3 Concluding remarks

Brain dynamics shows a complex organization at many spatiotemporal scales (Deco et al., 2011; Perdikis et al., 2011), a proper characterization of temporal scales could provide some guidance for

experimental steps. Whole-brain computational modeling has played an important role for understanding intrinsic brain dynamics (Cabral et al., 2014), and neuropsychiatric disorders (Deco and Kringelbach, 2014). On the other hand, computational models combined with the extraction of spatiotemporal features could thus play a significant role not only for a better understanding of intrinsic brain dynamics (Deco et al., 2019) , but also opens up to get a personalized care of neuropsychiatric disruptions (Falcon, Jirsa, et al., 2016). Besides, subject-based perspective may improve some treatments by predicting the outcome, but also more generally in the discovery of biomarkers. In general terms, the application of brain modeling for an individualized medicine have demonstrated a high relevance for clinical interventions of epileptic patients (V. K. Jirsa et al., 2017) and stroke recovery (Falcon, Riley, et al., 2016).

In summary, computational methods, such as whole-brain modelling (Deco and Kringelbach, 2014; Deco et al., 2008) and machine learning (Vu et al., 2018), complement traditional neuroimaging techniques to study brain dynamics at different timescales. However, future work is needed to study brain dynamics while performing cognitive processes and possible disruptions of such dynamics in clinical population. Overall, we believe our work opens future benefits to base medical practices on the individual characteristics of patients (Vogenberg et al., 2010), as well as for predicting the course of neuropsychiatric disorders (Ozomaro et al., 2013).

Bibliography

Matthews, P. M., Edison, P., Geraghty, O. C., & Johnson, M. R. (2014). The emerging agenda of stratified medicine in neurology. *Nature Reviews Neurology*, *10*(1), 15–26.

Hamburg, M. A., & Collins, F. S. (2010). The Path to Personalized Medicine. *New England Journal of Medicine*, *363*(4), 301–304
doi: 10.1056/NEJMp1006304.

Polivka, J., Polivka Jr, J., Krakorova, K., Peterka, M., & Topolcan, O. (2016). Current status of biomarker research in neurology. *The EPMA journal*, *7*(1), 14.

Brammer, M. (2009). The role of neuroimaging in diagnosis and personalized medicine–current position and likely future directions. *Dialogues in clinical neuroscience*, *11*(4), 389–396.

Deco, G., Jirsa, V. K., & McIntosh, A. R. (2011). Emerging concepts for the dynamical organization of resting-state activity in the brain. *Nat Rev Neurosci*, *12*(1), 43–56
10.1038/nrn2961.

Markram, H. (2013). Seven challenges for neuroscience. *Functional Neurology*, *28*(3), 145–151.

Haines, D. E. (2012). *Fundamental Neuroscience for Basic and Clinical Applications E-Book: with STUDENT CONSULT Online Access*. Elsevier Health Sciences.

Squire, L., Berg, D., Bloom, F., du Lac, S., Ghosh, A., & Spitzer, N. (2013). *Fundamental Neuroscience*. Elsevier Science.

Bandettini, P. A. (2009). Functional MRI limitations and aspirations. *Neural Correlates of Thinking* (pp. 15–38). Springer.

Glover, G. H. (2011). Overview of functional magnetic resonance imaging. *Neurosurgery Clinics*, *22*(2), 133–139.

Bressler, S. L., & Kelso, J. (2001). Cortical coordination dynamics and cognition. *Trends in Cognitive Sciences*, *5*(1), 26–36.

Jirsa, V. K. (2004). Connectivity and dynamics of neural information processing. *Neuroinformatics*, *2*(2), 183–204.

Bressler, S. L. (2002). Understanding Cognition Through Large-Scale Cortical Networks. *Current Directions in Psychological Science*, *11*(2), 58–61
doi: 10.1111/1467-8721.00168.

Johansen-Berg, H., & Rushworth, M. F. S. (2009). Using diffusion imaging to study human connectional anatomy. *Annual review of neuroscience*, *32*, 75–94.

Hagmann, P., Cammoun, L., Gigandet, X., Gerhard, S., Grant, P. E., Wedeen, V., Meuli, R., Thiran, J.-P., Honey, C. J., & Sporns, O. (2010). MR connectomics: Principles and challenges. *Journal of neuroscience methods*, *194*(1), 34–45.

Greicius, M. D., Krasnow, B., Reiss, A. L., & Menon, V. (2003). Functional connectivity in the resting brain: A network analysis of the default mode hypothesis. *Proceedings of the National Academy of Sciences*, *100*(1), 253 LP –258.

Deco, G., Hartevelt, T. V., Fernandes, H. M., Stevner, A., & Kringelbach, M. (2017). The most relevant human brain regions for functional connectivity: Evidence for a dynamical workspace of binding nodes from whole-brain computational modelling. *NeuroImage*, *146*, 197–210.

Lenartowicz, A., & Poldrack, R. A. (2010). Brain Imaging. In G. F. Koob, M. L. Moal, & R. F. B. T. E. o. B. N. Thompson (Eds.). Academic Press.

Fox, M. D., & Raichle, M. E. (2007). Spontaneous fluctuations in brain activity observed with functional magnetic resonance imaging. *Nature Reviews Neuroscience*, *8*(9), 700–711.

Damoiseaux, J. S., Rombouts, S. A. R. B., Barkhof, F., Scheltens, P., Stam, C. J., Smith, S. M., & Beckmann, C. F. (2006). Consistent resting-state networks across healthy subjects. *Proceedings of the National Academy of Sciences of the United States of America*, *103*(37), 13848–13853.

Pannunzi, M., Hindriks, R., Bettinardi, R. G., Wenger, E., Lisofsky, N., Martensson, J., Butler, O., Filevich, E., Becker, M., Lochstet, M., Kühn, S., & Deco, G. (2017). Resting-state fMRI correlations: From link-wise unreliability to whole brain stability. *NeuroImage*, *157*, 250–262.

Shah, N. J., Arrubla, J., Rajkumar, R., Farrher, E., Mauler, J., Kops, E. R., Tellmann, L., Scheins, J., Boers, F., Dammers, J., Sripad, P., Lerche, C., Langen, K. J., Herzog, H., & Neuner, I. (2017). Multimodal Fingerprints of Resting State Networks as assessed by Simultaneous Trimodal MR-PET-EEG Imaging. *Scientific Reports*, *7*(1), 6452.

Dickerson, B. C., Stoub, T. R., Shah, R. C., Sperling, R. A., Killiany, R. J., Albert, M. S., Hyman, B. T., Blacker, D., & DeToledo-Morrell, L. (2011). Alzheimer-signature MRI biomarker predicts AD dementia in cognitively normal adults. *Neurology*, *76*(16), 1395 LP –1402.

Jirsa, V. K., Proix, T., Perdikis, D., Woodman, M. M., Wang, H., Gonzalez-Martinez, J., Bernard, C., Bénar, C., Guye, M., Chauvel, P., & Bartolomei, F. (2017). The Virtual Epileptic Patient: Individualized whole-brain models of epilepsy spread. *NeuroImage*, *145*, 377–388.

Idrobo, A. H. (2017). Ensembles of models in fMRI : stable learning in large-scale settings.

Deco, G., & Kringelbach, M. L. (2014). Great Expectations: Using Whole-Brain Computational Connectomics for Understanding Neuropsychiatric Disorders. *Neuron*, *84*(5), 892–905.

Deco, G., Jirsa, V. K., Robinson, P. A., Breakspear, M., & Friston, K. (2008). The Dynamic Brain: From Spiking Neurons to Neural Masses and Cortical Fields. *PLoS Computational Biology*, *4*(8), e1000092.

Fan, X., & Markram, H. (2019). A Brief History of Simulation Neuroscience. *Frontiers in Neuroinformatics*, *13*, 32.

Wass, S. (2011). Distortions and disconnections: Disrupted brain connectivity in autism. *Brain and Cognition*, *75*(1), 18–28.

Mainen, Z. F., & Sejnowski, T. J. (1995). Reliability of spike timing in neocortical neurons. *Science*, *268*(5216), 1503–1506.

Deco, G., Cruzat, J., & Kringelbach, M. L. (2019). Brain songs framework used for discovering the relevant timescale of the human brain. *Nature Communications*, *10*(1), 583.

Harris, K. D., Csicsvari, J., Hirase, H., Dragoi, G., & Buzsaki, G. (2003). Organization of cell assemblies in the hippocampus. *Nature*, *424*(6948), 552–556 10.1038/nature01834.

Hebb, D. O. (1949). *The Organization of Behavior: a neuropsychological theory*. Psychology Press.

Sakurai, Y. (1999). How do cell assemblies encode information in the brain? *Neuroscience & Biobehavioral Reviews*, *23*(6), 785–796.

Glaser, J. I., Benjamin, A. S., Farhoodi, R., & Kording, K. P. (2019). The roles of supervised machine learning in systems neuroscience. *Progress in Neurobiology*, *175*, 126–137.

Lemm, S., Blankertz, B., Dickhaus, T., & Müller, K. R. (2011). Introduction to machine learning for brain imaging. *NeuroImage*, *56*(2), 387–399.

Varoquaux, G., & Thirion, B. (2014). How machine learning is shaping cognitive neuroimaging. *GigaScience*, *3*(1), 28.

Vacariu, G., & Vacariu, M. (2013). Troubles with Cognitive Neuroscience. *Philosophia Scientiae*, *17*(2), 151–170.

Carlson, T., Goddard, E., Kaplan, D. M., Klein, C., & Ritchie, J. B. (2018). Ghosts in machine learning for cognitive neuroscience: Moving from data to theory. *NeuroImage*, *180*, 88–100.

Holzinger, A. (2014). Trends in Interactive Knowledge Discovery for Personalized Medicine: Cognitive Science meets Machine Learnin. *The IEEE intelligent informatics bulletin*, *15*(1), 6–14.

Janssen, R. J., Mourão-Miranda, J., & Schnack, H. G. (2018). Making Individual Prognoses in Psychiatry Using Neuroimaging and Machine Learning. *Biological Psychiatry: Cognitive Neuroscience and Neuroimaging*, *3*(9), 798–808.

Ozomaro, U., Wahlestedt, C., & Nemeroff, C. B. (2013). Personalized medicine in psychiatry: problems and promises. *BMC Medicine*, *11*(1), 132.

Mulert, C., Pogarell, O., & Hegerl, U. (2008). Simultaneous EEG-fMRI: Perspectives in psychiatry. http://journals.sagepub.com/doi/10.1177/155005940803900207

Steyrl, D., Patz, F., Krausz, G., Edlinger, G., & Müller-Putz, G. R. (2015). Reduction of EEG artifacts in simultaneous EEG-fMRI: Reference layer adaptive filtering (RLAF). *2015 37th Annual International Conference of the IEEE Engineering in Medicine and Biology Society (EMBC)*, 3803–3806.

Strimbu, K., & Tavel, J. A. (2010). What are biomarkers? *Current opinion in HIV and AIDS*, *5*(6), 463–466.

Filiou, M. D., & Turck, C. W. (2011). Chapter 1 - General overview: Biomarkers in neuroscience research. In P. C. Guest & S. Bahn (Eds.), *Biomarkers of Neurological and Psychiatric Disease* (pp. 1–17). Academic Press.

Akzhigitov, A. B., Burnaev, E., Kondratyeva, E., Sushchinskaya, S., Sharaev, M., Andreev, A., Artemov, A., & Renat. (2018). Machine Learning pipeline for discovering neuroimaging-based biomarkers in neurology and psychiatry. *arXIv preprint arXIv:1804.10163*.

Deco, G., Ponce-Alvarez, A., Hagmann, P., Romani, G. ., Mantini, D., & Corbetta, M. (2014). How local excitation-inhibition

ratio impacts the whole brain dynamics. *The Journal of neuroscience*, *34*(23), 7886–98.

Zuo, X.-N., Anderson, J. S., Bellec, P., Birn, R. M., Biswal, B. B., Blautzik, J., Breitner, J. C. S., Buckner, R. L., Calhoun, V. D., Castellanos, F. X., Chen, A., Chen, B., Chen, J., Chen, X., Colcombe, S. J., Courtney, W., Craddock, R. C., Di Martino, A., Dong, H.-M., … Milham, M. P. (2014). An open science resource for establishing reliability and reproducibility in functional connectomics. *Scientific Data*, *1*, 140049.

Senden, M., Reuter, N., van den Heuvel, M. P., Goebel, R., & Deco, G. (2017). Cortical rich club regions can organize state-dependent functional network formation by engaging in oscillatory behavior. *NeuroImage*, *146*, 561–574.

Poldrack, R. A., Congdon, E., Triplett, W., Gorgolewski, K. J., Karlsgodt, K. H., Mumford, J. A., Sabb, F. W., Freimer, N. B., London, E. D., Cannon, T. D., & Bilder, R. M. (2016). A phenome-wide examination of neural and cognitive function. *Scientific data*, *3*, 160110.

Kirchner, W. K. (1958). Age differences in short-term retention of rapidly changing information.

Eriksen, B. A., & Eriksen, C. W. (1974). Effects of noise letters upon the identification of a target letter in a nonsearch task. *Perception & Psychophysics*, *16*(1), 143–149

Cited By :3651 Export Date: 12 September 2019.

Shepard, R. N., & Metzler, J. (1971). Mental Rotation of Three-Dimensional Objects. *Science*, *171*(3972), 701–703.

Flowers, K. A., & Robertson, C. (1985). The effect of Parkinson's disease on the ability to maintain a mental set. *Journal of Neurology, Neurosurgery & Psychiatry*, *48*(6), 517 LP –529.

Messé, A., Rudrauf, D., Benali, H., & Marrelec, G. (2014). Relating Structure and Function in the Human Brain: Relative Contributions of Anatomy, Stationary Dynamics, and Non-stationarities. *PLOS Computational Biology*, *10*(3), 1–9.

Hagmann, P., Cammoun, L., Gigandet, X., Meuli, R., Honey, C. J., Wedeen, V. J., & Sporns, O. (2008). Mapping the Structural Core of Human Cerebral Cortex. *PLOS Biology*, *6*(7), 1–15.

Yan, C. G., Wang, X. D., Zuo, X. N., & Zang, Y. F. (2016). DPABI: Data Processing & Analysis for (Resting-State) Brain Imaging. *Neuroinformatics*, *14*(3), 339–351.

Behzadi, Y., Restom, K., Liau, J., & Liu, T. T. (2007). A component based noise correction method (CompCor) for BOLD and perfusion based fMRI. *NeuroImage*, *37*(1), 90–101.

Reuter, M., Schmansky, N. J., Rosas, H. D., & Fischl, B. (2012). Within-subject template estimation for unbiased longitudinal image analysis. *NeuroImage*, *61*(4), 1402–1418.

Desikan, R. S., Ségonne, F., Fischl, B., Quinn, B. T., Dickerson, B. C., Blacker, D., Buckner, R. L., Dale, A. M., Maguire, R. P., Hyman, B. T., Albert, M. S., & Killiany, R. J. (2006). An automated labeling system for subdividing the human cerebral cortex on MRI scans into gyral based regions of interest. *NeuroImage*, *31*(3), 968–980.

Patel, A. X., & Bullmore, E. T. (2016). A wavelet-based estimator of the degrees of freedom in denoised fMRI time series for prob-

abilistic testing of functional connectivity and brain graphs. *NeuroImage*, *142*, 14–26.

Esteban, O., Markiewicz, C. J., Blair, R. W., Moodie, C. A., Isik, A. I., Erramuzpe, A., Kent, J. D., Goncalves, M., DuPre, E., Snyder, M., Oya, H., Ghosh, S. S., Wright, J., Durnez, J., Poldrack, R. A., & Gorgolewski, K. J. (2019). fMRIPrep: a robust preprocessing pipeline for functional MRI. *Nature Methods*, *16*(1), 111–116.

Gorgolewski, K., Burns, C., Madison, C., Clark, D., Halchenko, Y., Waskom, M., & Ghosh, S. (2011). Nipype: A Flexible, Lightweight and Extensible Neuroimaging Data Processing Framework in Python. *Frontiers in Neuroinformatics*, *5*, 13.

Tustison, N. J., Avants, B. B., Cook, P. A., Zheng, Y., Egan, A., Yushkevich, P. A., & Gee, J. C. (2010). N4ITK: Improved N3 Bias Correction. *IEEE Transactions on Medical Imaging*, *29*(6), 1310–1320.

Dale, A. M., Fischl, B., & Sereno, M. I. (1999). Cortical Surface-Based Analysis: I. Segmentation and Surface Reconstruction. *NeuroImage*, *9*(2), 179–194.

Klein, A., Ghosh, S. S., Bao, F. S., Giard, J., Häme, Y., Stavsky, E., Lee, N., Rossa, B., Reuter, M., Chaibub Neto, E., & Keshavan, A. (2017). Mindboggling morphometry of human brains. *PLOS Computational Biology*, *13*(2), e1005350.

Fonov, V. S., Evans, A. C., McKinstry, R. C., Almli, C. R., & Collins, D. L. (2009). Unbiased nonlinear average age-appropriate brain templates from birth to adulthood. *NeuroImage*, *47*, S102.

Avants, B. B., Epstein, C. L., Grossman, M., & Gee, J. C. (2008). Symmetric diffeomorphic image registration with cross-correlation: Evaluating automated labeling of elderly and neurodegenerative brain. *Medical Image Analysis*, *12*(1), 26–41 Special Issue on The Third International Workshop on Biomedical Image Registration – WBIR 2006.

Zhang, Y., Jones, C., & Dickman, M. B. (2001). Identification of differentially expressed genes following treatment of monkey kidney cells with the mycotoxin fumonisin B1. *Food and Chemical Toxicology*, *39*(1), 45–53.

Cox, R.W. and Hyde, J. (1997). Software tools for analysis and visualization of fMRI data. *NMR Biomed*, *10*, 171–178.

Jenkinson, M., Bannister, P., Brady, M., & Smith, S. (2002). Improved Optimization for the Robust and Accurate Linear Registration and Motion Correction of Brain Images. *NeuroImage*, *17*(2), 825–841.

Huntenburg, J. (2014). *Evaluating nonlinear coregistration of BOLD EPI and T1w images* (Doctoral dissertation). Freie Universität Berlin.

Wang, S., Peterson, D. J., Gatenby, J. C., Li, W., Grabowski, T. J., & Madhyastha, T. M. (2017). Evaluation of Field Map and Nonlinear Registration Methods for Correction of Susceptibility Artifacts in Diffusion MRI. *Frontiers in Neuroinformatics*, *11*, 17.

Treiber, J. M., White, N. S., Steed, T. C., Bartsch, H., Holland, D., Farid, N., McDonald, C. R., Carter, B. S., Dale, A. M., & Chen, C. C. (2016). Characterization and Correction of Geo-

metric Distortions in 814 Diffusion Weighted Images. *PLOS ONE*, *11*(3), 1–9.

Greve, D. N., & Fischl, B. (2009). Accurate and robust brain image alignment using boundary-based registration. *NeuroImage*, *48*(1), 63–72.

Lanczos, C. (1964). Evaluation of Noisy Data. *Journal of the Society for Industrial and Applied Mathematics Series B Numerical Analysis*, *1*(2), 76–85.

Power, J. D., Mitra, A., Laumann, T. O., Snyder, A. Z., Schlaggar, B. L., & Petersen, S. E. (2014). Methods to detect, characterize, and remove motion artifact in resting state fMRI. *NeuroImage*, *84*, 320–341.

Pruim, R. H. R., Mennes, M., van Rooij, D., Llera, A., Buitelaar, J. K., & Beckmann, C. F. (2015). ICA-AROMA: A robust ICA-based strategy for removing motion artifacts from fMRI data. *NeuroImage*, *112*, 267–277.

Aquino, K. M., Fulcher, B. D., Parkes, L., Sabaroedin, K., & Fornito, A. (2020). Identifying and removing widespread signal deflections from fMRI data: Rethinking the global signal regression problem. *NeuroImage*, *212*, 116614.

Deco, G., & Rolls, E. T. (2005). Neurodynamics of Biased Competition and Cooperation for Attention: A Model With Spiking Neurons. *Journal of Neurophysiology*, *94*(1), 295–313 doi: 10.1152/jn.01095.2004.

Wilson, M. T., Sleigh, J. W., Steyn-Ross, D. A., & Steyn-Ross, M. L. (2006). General Anesthetic-induced Seizures Can Be Explained by a Mean-field Model of Cortical Dynamics. *Anesthesiology*, *104*(3), 588–593.

Wong, K.-F., & Wang, X.-J. (2006). A Recurrent Network Mechanism of Time Integration in Perceptual Decisions. *The Journal of Neuroscience*, *26*(4), 1314 LP –1328.

Brunel, N., & Wang, X. J. (2001). Effects of neuromodulation in a cortical network model of object working memory dominated by recurrent inhibition. *Journal of Computational Neuroscience*, *11*(1), 63–85.

Deco, G., & Kringelbach, M. (2016). Metastability and Coherence: Extending the Communication through Coherence Hypothesis Using a Whole-Brain Computational Perspective. *Trends in Neurosciences*, *39*(6), 432.

Friston, K., Harrison, L., & Penny, W. (2003). Dynamic causal modelling. *NeuroImage*, *19*(4), 1273–1302.

Stephan, K. E., Weiskopf, N., Drysdale, P. M., Robinson, P. A., & Friston, K. J. (2007). Comparing hemodynamic models with DCM (2007/08/11). *NeuroImage*, *38*(3), 387–401.

Biswal, B., Zerrin Yetkin, F., Haughton, V. M., & Hyde, J. S. (1995). Functional connectivity in the motor cortex of resting human brain using echo-planar mri. *Magnetic Resonance in Medicine*, *34*(4), 537–541.

Glerean, E., Salmi, J., Lahnakoski, J. M., Jääskeläinen, I. P., & Sams, M. (2012). Functional Magnetic Resonance Imaging Phase Synchronization as a Measure of Dynamic Functional Connectivity. *Brain Connectivity*, *2*(2), 91–101.

Achard, S., Salvador, R., Whitcher, B., Suckling, J., & Bullmore, E. (2006). A resilient, low-frequency, small-world human brain functional network with highly connected association cortical hubs. *Journal of Neuroscience*, *26*(1), 63–72.

Deco, G., Kringelbach, M. L., Jirsa, V. K., & Ritter, P. (2017). The dynamics of resting fluctuations in the brain: Metastability and its dynamical cortical core. *Scientific Reports*, *7*(1), 1–14.

Lopes-dos-Santos, V., Conde-Ocazionez, S., Nicolelis, M. A., Ribeiro, S. T., & Tort, A. B. (2011). Neuronal assembly detection and cell membership specification by principal component analysis. *PLoS ONE*, *6*(6).

Lopes-dos-Santos, V., Ribeiro, S., & Tort, A. B. (2013). Detecting cell assemblies in large neuronal populations. *Journal of Neuroscience Methods*, *220*(2), 149–166.

Tagliazucchi, E., Balenzuela, P., Fraiman, D., & Chialvo, D. R. (2012). Criticality in large-scale brain FMRI dynamics unveiled by a novel point process analysis. *Frontiers in physiology*, *3*, 15.

Deco, G., & Kringelbach, M. (2017). Hierarchy of Information Processing in the Brain: A Novel 'Intrinsic Ignition' Framework. *Neuron*, *94*(5), 961–968.

Marchenko, V. A., & Pastur, L. A. (1967). Distribution of Eigenvalues for Some Sets of Random Matrices. *Mathematics of the USSR-Sbornik*, *1*(4), 457–483.

Peyrache, A., Benchenane, K., Khamassi, M., Wiener, S. I., & Battaglia, F. P. (2010). Principal component analysis of ensemble recordings reveals cell assemblies at high temporal resolution. *Journal of Computational Neuroscience*, *29*(1), 309–325.

Stulz, S. B., Insabato, A., Deco, G., Gilson, M., & Senden, M. (2018). Comparing Task-Relevant Information Across Differ-

ent Methods of Extracting Functional Connectivity. *bioRxiv*, 509059.

Pedregosa, F., Varoquaux, G., Gramfort, A., Michel, V., Thirion, B., Grisel, O., Blondel, M., Prettenhofer, P., Weiss, R., Dubourg, V., Perrot, M., & Duchesnay, É. (2011). Scikit-learn: Machine learning in Python. *Journal of Machine Learning Research*, *12*, 2825–2830.

Koenig, T., Studer, D., Hubl, D., Melie, L., & Strik, W. K. (2005). Brain connectivity at different time-scales measured with EEG. *Philosophical Transactions of the Royal Society B: Biological Sciences*, *360*(1457), 1015–1024 doi: 10.1098/rstb.2005.1649.

Lehmann, D., Strik, W. K., Henggeler, B., Koenig, T., & Koukkou, M. (1998). Brain electric microstates and momentary conscious mind states as building blocks of spontaneous thinking: I. Visual imagery and abstract thoughts. *International journal of psychophysiology : official journal of the International Organization of Psychophysiology*, *29*(1), 1–11.

Del Cul, A., Baillet, S., & Dehaene, S. (2007). Brain Dynamics Underlying the Nonlinear Threshold for Access to Consciousness. *PLOS Biology*, *5*(10), 1–16.

van Vugt, B., Dagnino, B., Vartak, D., Safaai, H., Panzeri, S., Dehaene, S., & Roelfsema, P. R. (2018). The threshold for conscious report: Signal loss and response bias in visual and frontal cortex. *Science*, *360*(6388), 537 LP –542.

Dehaene, S., & Changeux, J.-P. (2011). Experimental and Theoretical Approaches to Conscious Processing. *Neuron*, *70*(2), 200–227.

Logothetis, N. K. (2008). What we can do and what we cannot do with fMRI. *Nature*, *453*(7197), 869–878.

Cabral, J., Kringelbach, M. L., & Deco, G. (2014). Exploring the network dynamics underlying brain activity during rest. *Progress in Neurobiology*, *114*, 102–131.

Falcon, M. I., Jirsa, V., & Solodkin, A. (2016). A new neuroinformatics approach to personalized medicine in neurology: The Virtual Brain. *Current opinion in neurology*, *29*(4), 429–436.

Falcon, M. I., Riley, J. D., Jirsa, V., McIntosh, A. R., Chen, E. E., & Solodkin, A. (2016). Functional Mechanisms of Recovery after Chronic Stroke: Modeling with the Virtual Brain. *eNeuro*, *3*(2), ENEURO.0158–15.2016.

Vu, M.-A. T., Adalı, T., Ba, D., Buzsáki, G., Carlson, D., Heller, K., Liston, C., Rudin, C., Sohal, V. S., Widge, A. S., Mayberg, H. S., Sapiro, G., & Dzirasa, K. (2018). A Shared Vision for Machine Learning in Neuroscience (2018/01/26). *The Journal of neuroscience : the official journal of the Society for Neuroscience*, *38*(7), 1601–1607.

Vogenberg, F. R., Isaacson Barash, C., & Pursel, M. (2010). Personalized medicine: part 1: evolution and development into theranostics. *P & T : a peer-reviewed journal for formulary management*, *35*(10), 560–576.

Huys, R., Perdikis, D., & Jirsa, V. K. (2014). Functional architectures and structured flows on manifolds: a dynamical framework for motor behavior. *Psychological review*, *121*(3), 302–336.

Perdikis, D., Huys, R., & Jirsa, V. K. (2011). Time Scale Hierarchies in the Functional Organization of Complex Behaviors. *PLOS Computational Biology*, *7*(9), 1–18.

Woodman, M., Perdikis, D., Pillai, A. S., Dodel, S., Huys, R., Bressler, S., & Jirsa, V. (2011). Building neurocognitive networks with a distributed functional architecture. *Advances in experimental medicine and biology*, *718*, 101–109.

Jirsa, V. K., Stacey, W. C., Quilichini, P. P., Ivanov, A. I., & Bernard, C. (2014). On the nature of seizure dynamics. *Brain*, *137*(8), 2210–2230.

Spencer, K. M., Nestor, P. G., Perlmutter, R., Niznikiewicz, M. A., Klump, M. C., Frumin, M., Shenton, M. E., & McCarley, R. W. (2004). Neural synchrony indexes disordered perception and cognition in schizophrenia. *Proceedings of the National Academy of Sciences*, *101*(49), 17288–17293.

Michels, L., Bucher, K., Lüchinger, R., Klaver, P., Martin, E., Jeanmonod, D., & Brandeis, D. (2010). Simultaneous EEG-fMRI during a Working Memory Task: Modulations in Low and High Frequency Bands. *PLOS ONE*, *5*(4), e10298.

Kringelbach, M. L., Lehtonen, A., Squire, S., Harvey, A. G., Craske, M. G., Holliday, I. E., Green, A. L., Aziz, T. Z., Hansen, P. C., Cornelissen, P. L., & Stein, A. (2008). A Specific and Rapid Neural Signature for Parental Instinct. *PLoS ONE*, *3*(2), e1664.

Kringelbach, M. L., McIntosh, A. R., Ritter, P., Jirsa, V. K., & Deco, G. (2015). The Rediscovery of Slowness: Exploring the Timing of Cognition. *Trends in Cognitive Sciences*, *19*(10), 616–628.

Phillips, W. A., & Silverstein, S. M. (2003). Convergence of biological and psychological perspectives on cognitive coordination

in schizophrenia. *Behavioral and Brain Sciences*, *26*(1), 65–82.

Phillips, J., Frances, A., Cerullo, M. A., Chardavoyne, J., Decker, H., First, M. D., Ghaemi, N., Greenberg, G., Hinderliter, A. C., Kinghorn, W. A., LoBello, S. G., Martin, E. B., Mishara, A. L., Paris, J., Pierre, J. M., Pies, R. W., Pincus, H. A., Porter, D., Pouncey, C., … Zachar, P. (2012). The six most essential questions in psychiatric diagnosis: a pluralogue part 3: issues of utility and alternative approaches in psychiatric diagnosis. *Philos Ethics Humanit Med*, *7*.

Deco, G., Ponce-Alvarez, A., Mantini, D., Romani, G. L., Hagmann, P., & Corbetta, M. (2013). Resting-State Functional Connectivity Emerges from Structurally and Dynamically Shaped Slow Linear Fluctuations. *The Journal of Neuroscience*, *33*(27), 11239 LP –11252.

Krajcovic, B., Fajnerova, I., Horacek, J., Kelemen, E., Kubik, S., Svoboda, J., & Stuchlik, A. (2019). Neural and neuronal discoordination in schizophrenia: From ensembles through networks to symptoms. *Acta Physiologica*, *226*(4), e13282.

Olypher, A. V., Klement, D., & Fenton, A. A. (2006). Cognitive Disorganization in Hippocampus: A Physiological Model of the Disorganization in Psychosis. *Journal of Neuroscience*, *26*(1), 158–168.

Dawson, K. A. (2004). Temporal organization of the brain: Neurocognitive mechanisms and clinical implications. *Brain and Cognition*, *54*(1), 75–94.

Northoff, G., Sandsten, K. E., Nordgaard, J., Kjaer, T. W., & Parnas, J. (2020). The Self and Its Prolonged Intrinsic Neural Timescale in Schizophrenia. *Schizophrenia Bulletin*.

Watanabe, T., Rees, G., & Masuda, N. (2019). Atypical intrinsic neural timescale in autism. *Elife*, *8*, e42256.

Northoff, G. (2016). Spatiotemporal psychopathology I: No rest for the brain's resting state activity in depression? Spatiotemporal psychopathology of depressive symptoms.

Northoff, G. (2018). The brain's spontaneous activity and its psychopathological symptoms – "Spatiotemporal binding and integration".

Fingelkurts, A. A., & Fingelkurts, A. A. (2019). Brain space and time in mental disorders: Paradigm shift in biological psychiatry. http://journals.sagepub.com/doi/10.1177/0091217418791438

Morcom, A. M., & Fletcher, P. C. (2007). Does the brain have a baseline? Why we should be resisting a rest.

Lytton, W. W., Arle, J., Bobashev, G., Ji, S., Klassen, T. L., Marmarelis, V. Z., Schwaber, J., Sherif, M. A., & Sanger, T. D. (2017). Multiscale modeling in the clinic: diseases of the brain and nervous system. *Brain Informatics*, *4*(4), 219–230.